Cell Communication and Signaling

RESEARCH

Open Access

Intramyocardial injection of pre-cultured endothelial progenitor cells and mesenchymal stem cells inside alginate/gelatin microspheres induced angiogenesis in infarcted rabbits

Hassan Amini[1,2], Çığır Biray Avci[3], Sajed Nazif Kerdar[4], Ayla Hassani[4], Meisam Amini[5], Narges Mardi[1], Sepideh Saghati[1], Maryam Taghavi Narmi[1], Leila Sabour Takanlou[3], Maryam Sabour Takanlou[3], Ali Baradar Khoshfetrat[4], Mohammad Nori[1], Shahriar Hashemzadeh[2] and Reza Rahbarghazi[1,6*†]

Abstract

Background Using several strategies, the stimulation of angiogenesis can alleviate the pathological complications of post-myocardial ischemia. Here, endothelial progenitor cells (EPCs) and mesenchymal stem cells (MSCs) were pre-cultured inside the alginate/gelatin (Alg/Gel) microspheres in the presence of SDF-1α for 7 days, and their angiogenesis potential was monitored in infarcted rabbits.

Methods The decapsulated cells were monitored in terms of cell dynamic growth and angiogenesis potential in vitro and after injection into ischemic myocardium in rabbits.

Results Based on the data, 7-day incubation inside the Alg/Gel microspheres led to the stimulation of angiogenesis profile (Ang-1↑, -2↑, Tie-2↑), migration (MMP-2↑, and −9↑), and autophagic response (Beclin-1↑, LC3↑, and p-62↓) in EPCs containing groups in the presence of SDF-1α. PCR array analysis revealed the expression of angiogenesis-related genes in the presence of SDF-1α. These features coincided with the stimulation of in vitro tubulogenesis properties in EPCs and EPCs + SDF-1α groups. The injection of cells from different groups into the infarcted rabbits led to the reduction of fibrotic area in ischemic myocardium in MSCs-bearing groups, and these effects were intensified in the presence of SDF-1α. Pre-treatment of EPCs and MSCs increased the recruited immune cells into the ischemic area within the myocardium. It was suggested that SDF-1α stimulated the local vascular density (CD31 capillaries, and α-SMA arterioles) in EPCs-bearing groups compared to MSCs and MSCs + SDF-1α groups.

†Reza Rahbarghazi contributed equally to this work.

*Correspondence:
Reza Rahbarghazi
Rezarahbardvm@gmail.com; rahbarghazir@tbzmed.ac.ir

Full list of author information is available at the end of the article

Conclusions These data indicate that pre-culture of EPCs and MSCs inside the Alg-based hydrogels can increase the regenerative potential of these cells, especially when exposed to stimulatory cytokines such as SDF-1α for the alleviation of ischemic changes.

Keywords Endothelial progenitor cells, Mesenchymal stem cells, Myocardial infarction, Angiogenesis, Rabbits

Introduction

Ischemic heart disease (IHD), especially myocardial infarction (MI), is a leading global cause of human mortality and occurs by partial or complete obstruction of coronary arteries to cardiac tissue. The progression of ischemia, necrotic changes, and aberrant remodeling can lead to heart failure [1, 2]. Current therapeutic protocols include monitoring specific lifestyle and surgical interventions, i.e., angioplasty, placing stents inside the afflicted vascular beds, and coronary artery bypass grafting (CABG) [3]. Unfortunately, these modalities cannot restore the function of the injured myocardium, and thus, alternative approaches with higher regenerative outcomes are mandatory in IHD patients.

The advent of stem cell therapy and tissue engineering technologies has revolutionized human medicine in the last years [4, 5]. Several studies have indicated that stem cells directly commit to various cell lineages or secrete diverse cytokines and growth factors with the potential to accelerate the healing process inside the injured sites [6, 7]. Among different underlying mechanisms regulated by stem cells and their secretome, the restoration of blood support into the ischemic myocardium can promote reparative tissue mechanisms, resulting in cardiac function and aberrant pathological changes [8]. Among different stem cell types used for several regenerative purposes, endothelial progenitor cells (EPCs) and mesenchymal stem cells (MSCs) have exhibited significant angiogenesis potential in IHD [9]. The increase of microvascular units within the infarct area is promoted by direct differentiation into vascular cells or the release of pro-angiogenesis factors (angiocrine) by MSCs and EPCs in different animal models [10–14]. Under pathological conditions, the release of inflammatory cytokines such as stromal cell-derived factor 1 alpha (SDF-1α) from the injured sites recruits bone marrow MSCs and EPCs via the activation of CXCR-4 signaling pathway, making them valid stem cell sources for different regenerative purposes [15, 16].

Despite the existence of these features, the intracoronary injection of stem cells can increase the possibility of microvascular plugging due to vasculitis and inflammatory response [17]. Besides, direct intramyocardial injection yields poor engraftment and survival rate in transplanted stem cells due to excessive mechanical stress during the injection time, high levels of free radicals and reactive substances at the site of injury, leading to reduced intramyocardial retention time after being transplanted into the cardiac tissue [18]. Commensurate with these statements, encapsulation of stem cells inside polymeric hydrogels has been introduced as a novel effective approach to increase the on-target delivery efficiency, reduce environmental stresses, and post-complications associated with direct cell injection. For instance, encapsulation can protect allogeneic stem cells from the direct activity of alloreactive immune cells, oxidative stress, and mechanical damage. On the other hand, the existence of several motifs within the hydrogel structures can improve stem cell attachment, phenotype acquisition, dynamic growth, differentiation, and regenerative properties [18, 19]. Of note, the formation of homogenous and/or heterogenous juxtacrine interaction between the encapsulated stem cells in the presence of certain growth factors such as SDF-1α can also facilitate their release into the targeted sites [20, 21]. For example, it was suggested that the co-administration of EPC- and SDF-1α-loaded polyethylene glycol hydrogel can stimulate cell retention and angiogenesis potential in animal models of cardiac diseases [22].

Of different substrates and composites used for stem cell encapsulation, it has been shown that the combination of alginate-gelatin (Alg/Gel) exhibits an excellent platform for 3D in vitro culture and transplantation into the target organs [23, 24]. Alg is a cytocompatible and biodegradable polysaccharide with 1–4 glycosidic bonds in its chemical structure. However, Alg alone is anionic and lacks appropriate cell adhesion properties, which necessitate the addition of an extracellular matrix (ECM) component for better regenerative outcomes [24]. The addition of Gel can increase the interaction between the supporting hydrogels and encapsulated cells by providing several adhesive motifs. These features can lead to morphological adaptation and physiological cell behavior [25, 26].

Here, in this study, we aimed to investigate the angiogenesis potential of EPCs and MSCs after being encapsulated inside the Alg/Gel microspheres in the presence of SDF-1α in a rabbit model of myocardial infarction after 30 days post-transplantation. Whether and how co-administration of EPCs plus MSCs pre-cultured for 7 days inside the Alg/Gel microspheres induced by ionic cross-linking can affect the angiogenesis potential is the subject of debate. We hope that the data from this study can help in the development and fabrication of sophisticated engineered hydrogels for obtaining better regenerative outcomes in IHD patients (Fig. 1).

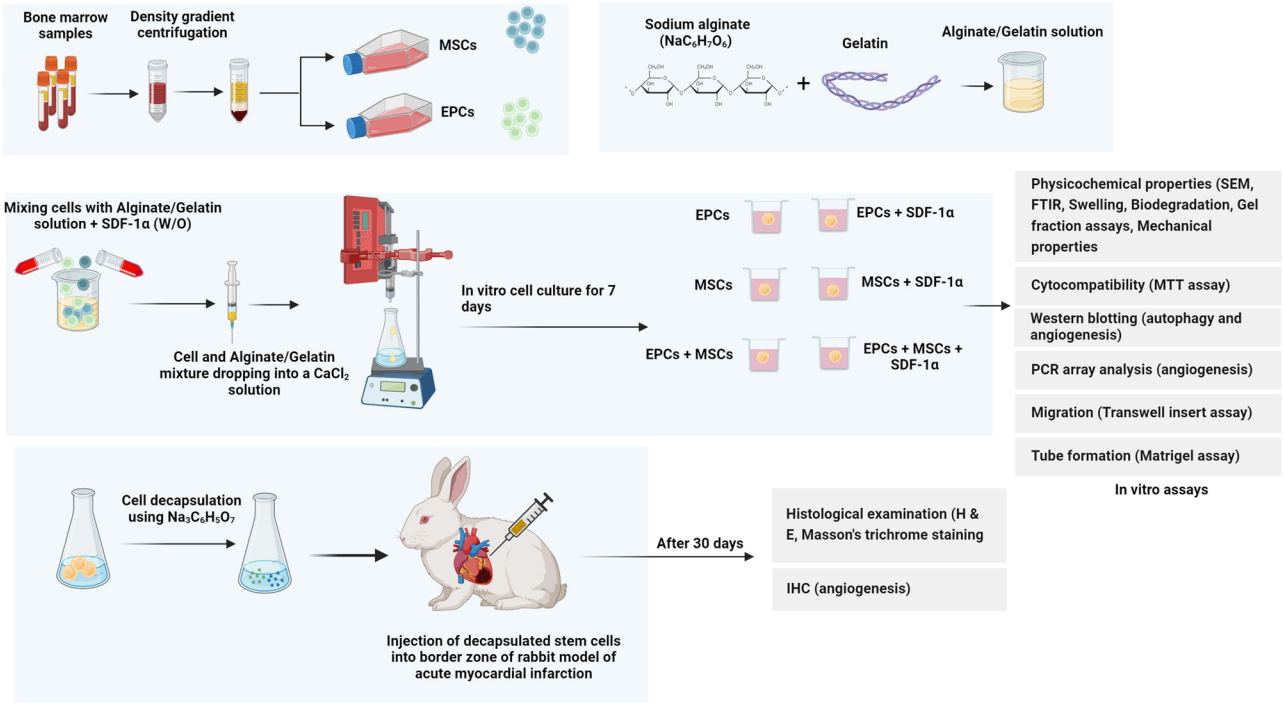

Fig. 1 The schematic diagram of the experimental procedure. EPCs and MSCs were isolated from human bone marrow samples. The synthesis of Alg/Gel hydrogel was done using $CaCl_2$ as a cross-linking agent. EPCs, MSCs, and/or their combination were incorporated into Alg/Gel microspheres in the presence and/or absence of SDF-1α using $CaCl_2$ solution under high-voltage conditions. After a 7-day in vitro culture, physicochemical assay, angiogenesis properties, migration capacity, and autophagy response were measured. For the in vivo assay, cells were decapsulated using tri-sodium citrate buffer and injected into a rabbit model of myocardial infarction. The histological changes, fibrosis, and angiogenesis properties were analyzed after 30 days post-transplantation

Materials and methods

Alg/Gel hydrogel synthesis protocol

In this study, Alg/Gel hydrogel was fabricated according to our previous study [27]. To this, sodium Alg with high guluronic acid contents (Molecular weight: 70 kDa; Kimica; Japan) was cross-linked using 0.2 M $CaCl_2$ with porcine cutaneous Gel (Sigma-Aldrich) to yield a polymeric network containing 1% (w/v) Alg and 1.125% (w/v) Gel. Before hydrogel synthesis, Alg was disinfected using 70% EtOH solution and washed several times with sterile Ca^{2+}-free Krebs Ringer HEPES-buffered saline (CF-KRH, pH = 7.2–7.4) inside the laminar hood.

FT-IR analysis

Using an FT-IR spectrophotometer (TENSOR 27, Germany) and infrared spectra within the range of 500–4000 cm-1 with a resolution of 4 cm-1 and 24 scans, the chemical structure and functional groups of Alg/Gel hydrogel were monitored.

Swelling and gel fraction

Cylinder-shaped hydrogels with a diameter of 1 cm and a height of 10 mm were fabricated through the process of pouring the Alg/Gel mixture into molds. To solidify the hydrogel, the molds containing Alg/Gel hydrogels were incubated in 0.2 M $CaCl_2$ solution. After being gelled, Alg/Gel hydrogels were weighed (W_I) and immersed in PBS at 37 °C for 24, 48, 72, and 96 h. At each time point, hydrogels were removed from PBS, dried using adsorbent papers, and weighed (W_f), and the swelling rate was measured using the following formula;

$$\text{Swelling ratio } (\%) = \left(\frac{W_f - W_I}{W_I}\right) \times 100$$

To calculate gel fraction, freeze-dried samples were incubated in deionized water for 48 h at room temperature. Therefore, samples were placed inside a vacuum oven at 70 °C for 24 h. The gel fraction (%) was measured using the following formula;

$$\text{Gel fraction } (\%) = \frac{W_d}{W_s} \times 100$$

Where W_s shows initial sample weights and W_d correlates with the weight of a dried, non-soluble portion of the specimen after the removal of water. This assay was done in sexaplicate.

Biodegradation rate

Alg/Gel gels with an initial weight of 0.65 g (W_i) were incubated in PBS supplemented with 1 mg/ml lysozyme (Cat no: 62970; Sigma-Aldrich). The degradation rate was followed by removing the hydrogels in PBS on days 0, 2, 4, 6, 8, 10, and 12. Afterward, samples were freeze-dried and subsequently weighed. The degradation rate was determined using the following equation from three separate samples for each group;

$$\text{Degradation rate}\,(\%) = \left(\frac{W_i - W_d}{W_i}\right) \times 100$$

W_d and W_i are associated with samples' weights at each time and initial weights, respectively.

Mechanical properties

To monitor the compressive load of hydrogels, the polymer solutions were solidified within PDMS cylinder molds (Height: 10 mm, and Diameter: 1 cm) ionic cross-linker as described above. The samples were analyzed at a velocity of 2.0 mm min^{-1}, utilizing apparatus for testing materials (Zwick/Roell Z010, Germany).

EPC and MSC isolation and expansion

In this study, human bone marrow samples were used for the isolation of EPCs and MSCs. In brief, the remnants of bone marrow (BM) samples were referred to Mardani Azar Children's Hospital, affiliated with Tabriz University of Medical Sciences. The informed consent process was done by the children's parents without any interference in the diagnosis process and therapeutic protocols. The remnant of samples referred to a laboratory setting was used for the isolation of EPCs and MSCs. The process of MSCs and EPCs was performed according to the previously published articles [28, 29]. BM samples were diluted with PBS at a ratio of 1:1, overlaid with an equal volume of Ficoll-Hypaque (Cat no: LSM-A; Capricorn Scientific) solution, and centrifuged at ~400 g for 20–30 min. The interphase mononuclear cells (MNCs) were carefully collected and washed twice with PBS to remove the unwanted remnants. Cells from different samples were pooled and divided into two main groups: EPCs and MSCs. For cell culture and isolation, MSCs were suspended in DMEM/LG supplemented with 10% fetal bovine serum (FBS; Gibco) and 1% penicillin/streptomycin (Pen/Strep; Biosera). After 24 h, the non-adherent cells were discarded, and the culture medium was replaced with fresh culture medium. For EPC isolation, MNCs were resuspended in DMEM/HG enriched with EGM-2 cocktail (Promocell), 10% FBS, and 1% Pen/Strep and precoated in fibronectin-coated flasks (Promocell). Cells were passaged using 0.25% Trypsin-EDTA solution (Gibco). In this study, cells between passages 3–6 were used for different studies.

EPC characterization

To this end, EPCs at passage three were cultured in 8 well chamber slides at an initial density of 1×10^4 per well and allowed to reach 70–80% confluence followed by incubation with 10 µg/ml Dil-labeled acetylated low-density lipoprotein (Dil-Ac-LDL; Cat no: 022 K; Cell Applications, Inc.) for 30 min [30]. Then, the cells were washed twice with PBS and fixed with pre-cooled 4% PFA for 20 min. The nuclei were stained with 1 µg/ml DAPI solution. Cells were imaged using fluorescence microscopy (Olympus).

Cell encapsulation inside alg/gel microspheres

EPCs and MSCs were trypsinized and washed three times with PBS. Cells were allocated into six groups as follows: EPCs, EPCs + SDF-1α, MSCs, MSCs + SDF-1α, EPCs + MSCs, EPCs + MSCs + SDF-1α. To encapsulate cells inside the Alg/Gel hydrogel, an electrostatic encapsulation method was applied using a high-voltage power supply (Vita Teb, Iran). In short, 1×10^6 cells were mixed with 1 ml of Alg/Gel solution in the presence or absence of 10 ng/m SDF-1α (Cat: no: 300–28 A; PeproTech). In MSC + EPCs groups, an equal number of both cell types (5×10^5) was used. Cell-laden hydrogels were transferred into 25G needles and dropped into a gelling bath containing 0.2 M $CaCl_2$. The distance between the syringe needle and the gelling bath was adjusted to 5 cm. After encapsulation, microspheres containing cells were washed three times with CFKRH buffer to remove free $CaCl_2$.

Scanning electron microscope (SEM)

After ionic gelation of cell-laden hydrogels, Alg/Gel composites were freeze-dried for 48 h. Using surgical blades, some samples were cut into small pieces and gold-sputtered. The existence of cells was carefully monitored using Field Emission Scanning Electron Microscopy (FESEM; MIRA3 TESCAN) under vacuum conditions and an accelerated 15 *kV*.

MTT assay

Cell-laden microspheres were cultured in DMEM/HG with 1% FBS and Pen-Strep for 7 days. After the completion of incubation time, the culture medium was discarded and replaced with 1 ml MTT (5 mg/ml; Sigma-Aldrich) solution at 37 °C for 24 h. After that, the culture medium was replaced with 1 ml DMSO solution and kept for 15 min. The OD values were read at 570 nm using a UV/Vis spectrophotometer (Cecil CE2501, Japan). OD values were normalized to the number of microspheres for each group.

Western blotting

To assess whether the encapsulation of EPCs, MSCs, and their combination with SDF-1α, or without SDF-1α can affect the angiogenesis potential, migration capacity, and autophagy response, cells were released from Alg/Gel hydrogel using trisodium citrate dihydrate (0.1 M; Cat no: AM0602948-517; Merck) and washed three times with PBS. Cells were collected and lysed using protein lysis buffer (NaCl, 50 mM Tris-HCl, 150 mM NP-40, and 0.1% SDS) containing anti-protease inhibitors. Samples were centrifuged at 4 °C with an average speed of 10,000 rpm for 20 min, and supernatants containing 10 µg protein were used for electrophoresis. Following electrophoresis on 10% SDS-PAGE, samples were transferred on PVFD membrane (Merck Millipore), blocked with 1% bovine serum albumin (BSA; Sigma-Aldrich), and incubated with a panel of antibodies against Ang-1, -2, Tie-2, MMP-2, -9, Beclin-1, LC3-II/I ratio, and p62 overnight at 4 °C. After that, membranes were washed three times with PBS containing 0.1% Tween-20 and incubated with appropriate HRP-conjugated secondary antibodies. The immunoreactive bands were detected using an ECL solution (Model: SB-14007; Sabz Biomedicals) and X-ray films. Relative protein levels were calculated using ImageJ software (NIH, ver. 1.4) compared to β-actin. All antibodies were purchased from Santa Cruz Biotechnology, Inc.

Table 1 Target factors used for monitoring angiogenesis potential

Genes	Primer Sequencing (5′-3′)
HPRT1	F- GACCAGTCAACAGGGGACAT
	R-GTGTCAATTATATCTTCCACAATCAAG
GAPDH	F- CGTAGCTCAGGCCTCAAGAC
	R- GCTGCGGGCTCAATTTATAG
ACTB	F- AGAGCTACGAGCTGCCTGAC
	R- CGTGGATGCCACAGGACT
HIF-1α	F- AGAGGTTGAGGGACGGAGAT
	R- GCACCAAGCAGGTCATAGGT
MMP-2	F- TAGCTGCTGGCTCACTGTGT
	R- CTTCAGCACAAACAGGTTGC
MMP-9	F- GAACCAATCTCACCGACAGG
	R- GCCACCCGAGTGTAACCATA
PECAM-1	F-TGAGTGGTGGGCTCAGATTG
	R-TGAGTCTAGGTCGGGGAGTG
IL-1β	F- AAACAGATGAAGTGCTCCTTCCAGG
	R- TGGAGAACACCACTTGTTGCTCCA
IL-6	F- GGTACATCCTCGACGGCATCT
	R- GT GCCTCTTTGCTGCTTTCAC
IL-8	F- AGGGCCAAGAGAATATCCGA
	R- ACTTGTGGATCCTGGCTAGC
NOTCH1	F-TGGACGACAACCAGAATGAG
	R-TCCTCGAACCGGAACTTCT
TGFBR1	F- GCAGACTTAGGACTGGCAGTAAG
	R- AGAACTTCAGGGGCCATGT
TIMP2	F- GTGGGTCCAAGGTCCTCAT
	R- CGAAGCCCCAGACACATAGT
TIMP3	F- CCTTCTGCAACTCCGACATC
	R- GCCCCTCCTTTACCAGCTT
TGFB1	F-AGTGGTTGAGCCGTGGAG
	R- GCACACACGTCACAACTGG
ERBB2	F- CAACTGCACCCACTCCTGT
	R- GCAGAGATGATGGACGTCAG
IFNA1	F- AACTCCCCTGATGAATGCGG
	R- AGTGTAAAGGTGCACATGACG
TNF	F- CAGCCTCTTCTCCTTCCTGAT
	R- GCCAGAGGGCTGATTAGAGA
VEGFA	F- CTACCTCCACCATGCCAAGT
	R- GATAGACATCCATGAACTTCACCA

Matrigel tubulogenesis assay

Functional angiogenesis behavior of EPCs, MSCs, and EPCs + MSCs exposed to SDF-1α was also monitored using the Matrigel assay. In short, 5×10^4 decapsulated cells were re-suspended in 500 µl DMEM/HG containing 1% FBS, and 1% Pen-Strep and placed in each well of 48-well plates pre-coated with 100 µl growth factor-reduced Matrigel (Corning). After 24 h, cells were imaged, and the tube length and area were calculated in 5 random high-power fields (HPF) using ImageJ software.

Transwell insert migration

To this end, 2×10^4 decapsulated cells were resuspended in a 200 µl culture medium and placed onto 8.0 µm pore polycarbonate membrane inserts. The bottom basolateral space was filled with 700–800 µl culture medium supplemented with 1% FBS. After 24 h, the number of migrated cells onto the bottom surface was imaged and counted in 10 random HPFs.

Angiogenesis array

qRT-PCR was performed for target genes including HIF-1α, MMP-2, MMP-9, PECAM-1, IL-1β, IL-6, IL-8, NOTCH1, TGFBR1, TIMP2, TIMP3, TGFB1, ERBB2, IFNA1 using RT2 SYBR Green qPCR Master Mix (Qiagen, 330503, Germany) via LightCycler 480 Instrument II (Roche, Germany). The gene expression level of each gene was normalized using HPRT1, GAPDH, and ACTB housekeeping genes, and data were analyzed utilizing the $2^{-\Delta\Delta CT}$ method to calculate fold changes in target gene expression (Table 1). The heatmap graphs were drawn based on the Log2 transformation of fold regulation.

Animal ethics

All experimental steps of the present study were approved by the local ethics committees of Tabriz University of Medical Sciences (IR.TBZMED.REC.1399.125) and the National Institute for Medical Research Development (NIMAD; IR.NIMAD.REC.1400.151). The current manuscript adheres to the ARRIVE guidelines. In this

study, 12-week-old male New Zealand white rabbits were purchased from the Razi Institute (Karaj, Iran). Animals were maintained under standard conditions in the animal house of Tabriz University of Medical Sciences inside standard cages and conditions (20 ± 2 °C, 12/12-hour light/dark cycle) with free access to chewing pellets and tap water. Animals were accommodated for 7 days before enrolling in the experimental procedure. In this study, rabbits were enrolled in different experimental groups with randomization.

Induction of the rabbit MI model and cell transplantation

The induction of MI in rabbits was done according to the previous study [31]. Animals received a combination of ketamine (50 mg/kg) and xylazine (5 mg/kg) via intramuscular injection. Following the induction of deep anesthesia, rabbits were placed in a dorsal position and intubated orally for tracheal ventilation using the anesthesia apparatus (Dräger Fabius, Germany). Vital parameters such as heartbeat, oxygen saturation, and electrocardiograms were carefully followed. Using a nonabsorbable suture (6 – 0 polypropylene), the left anterior descending coronary artery (LAD) was ligated in the region below the left auricle. Myocardial blanching and the elevation of the ST segment indicated successful myocardial ischemia. After 20–30 min post-LAD ligation, decapsulated rabbit MSCs, EPCs, or a mixture of MSCs and EPCs with/without SDF-1α pre-treatment inside the Alg/Gel (1×10^6) were resuspended in 100 µl normal saline and injected into the peripheral zone of the ischemic area in four sites. A total number of 1×10^6 cells in a ratio of 1:1 (5×10^5 MSCs plus 5×10^5 EPCs) was administered in the MSCs + EPCs groups. Before the thoracic wall suturing, the blood and biofluids were discharged using a chest tube to prevent pericardial fibrosis. After 30 days, rabbits were euthanized humanely using an overdose of ketamine and xylazine, and heart samples were subjected to different analyses. After heart sample collection, the left ventricles (LV) were sliced from the apex to the base and used for various analyses.

Histological examination

H & E, and masson's trichrome staining

To monitor the pathological conditions and the size of infarction in different groups, samples were fixed in a 10% buffered-formalin solution, and 5 µm-thick slices were prepared from paraffin-embedded blocks. The slices were stained using H & E and Masson's trichrome solution for general histological examination and monitoring fibrosis, respectively. For measuring fibrosis in each group, the area of the infarcted region was measured using ImageJ software (ver. 1.4; NIH), and the ratio of the infarcted region to the total area of each slice was calculated. Histological examinations were done by an expert pathologist who was not aware of the treatment groups and status of individual animals. The number of immune cells infiltrated into the border zone was also calculated using HPF.

Immunohistochemistry (IHC) staining

The angiogenesis status at the border of the infarcted zone was monitored after the injection of EPCs, MSCs, and EPCs + MSCs under different pre-treatment protocols using IHC staining. To this end, sections were deparaffinized and treated with hydrogen peroxide (3% v/v) for 20–30 min to blunt the endogenous peroxidase activity. Using autoclaving at 15 psi and citrate buffer (pH = 6.0) for 10 min, antigen retrieval was done. In the next step, the slices were permeabilized using 0.1% Triton-X 100 solution and incubated with antibodies against CD31 and α-SMA for 30–60 min at RT. After PBS washes, the EnVision + Dual Link System HRP kit (Dako, Denmark) was used for the detection of immunoreactive sites. Mayer's hematoxylin solution was used for background staining. To measure the microvascular density in the border zone, the number of $CD31^+$ capillaries and $\alpha\text{-SMA}^+$ arterioles was counted in 10 serial high-power fields (HPF) using Olympus microscopy.

Statical analysis

In the present experiment, data (mean ± SD) are evaluated using One-Way ANOVA with Tukey post hoc analysis. $p < 0.05$ was considered statistically significant. All experiments were conducted in triplicate, unless mentioned otherwise.

Results

EPC characterization

Fluorescence imaging revealed the ability of isolated EPCs to uptake Dil-Ac-LDL, in which the percent of Dil-Ac-LDL^+ cells reached ~ 87.3 ± 7.4%, indicating the efficiency of our protocol to isolate the EPCs (Fig. 2A).

FT-IR analysis

The functional groups, chemical bond formation, and rearrangement were analyzed using FT-IR spectroscopy (Fig. 2B). Data confirmed the existence of O-H bond stretching vibrations at 3400–3600 cm-1 in the Alg structure. The peak at the range of 2800–2927 cm-1 is attributed to the stretching vibrations of aliphatic C-H bonds. The vibrational mode associated with the asymmetric stretching of the O-C-O moiety exhibits a peak at 1618.80 cm-1. The spectral feature observed at 1418.21 cm-1 likely correlates with the bending vibration of the C-OH moiety, potentially with a contribution from the O-C-O group of the carboxylate [32, 33]. The weak spectral features observed at 1324.15 cm-1 and 1092.75 cm-1 regions were assigned to the vibrational

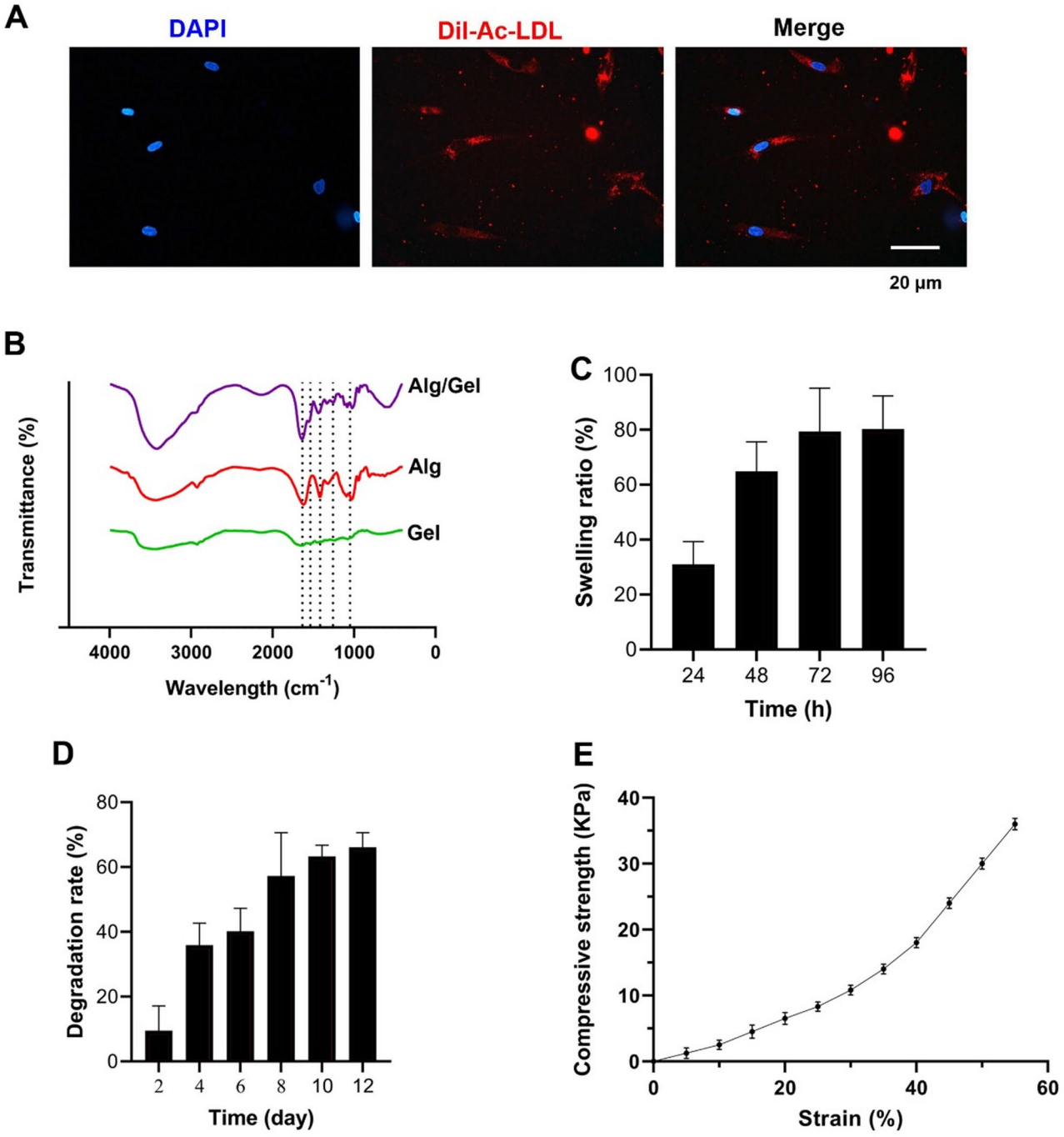

Fig. 2 Characterization of EPCs at passage 3 using Dil-Ac-LDL uptake (**A**). The cultured EPCs efficiently internalized red-colored Dil-Ac-LDL, indicating lipoprotein lipase activity (Blue: DAPI). FTIR (**B**). Swelling ratio (**C**; $n = 3$). Degradation rate (**D**; $n = 3$). Mechanical properties (**E;**$n = 3$)

modes of pyranose rings associated with C-C-H and O-C-H deformation, as well as C-O stretching, respectively. The existence of a peak at 1029.49 cm-1 is associated with the vibrational mode of C-O stretching. Of note, the spectral analysis indicated the presence of a peak at 944 cm-1, which can be attributed to the C-O stretching vibration of uronic acid residues. Additional signals located at 900 cm-1 and 813.22 cm-1 are integral to the asymmetric ring vibration of α-L-guluronic acid and the mannuronic acid residues, respectively [34, 35].

The absorption spectrum of Gel exhibits distinct absorption bands at 1300–1450 cm-1, which are attributed to carboxyl groups. The band at 1649.08 cm-1 corresponds to amide I and is related to the stretching vibrations of C = O and C-N. We also found bands at 1546.97 and 1451.11 cm-1 regions associated with amide

II because of N-H bending vibrations and C-N stretching vibrations. According to the data, the band located at 1239.40 cm-1 corresponds to amide III due to N-H bending vibrations and C-N stretching vibrations. The absorption band of O-H stretching vibration and N-H stretching of secondary amide in the spectrum of Gel were observed to shift to a lower wave number and peaked around 3439.41 cm-1, respectively. This phenomenon is possibly found due to the interaction with N-H. Additionally, the N-H out-of-plane wagging was observed at 701.90 cm-1 [36, 37] (Fig. 2B).

The spectral analysis Alg/Gel composite indicates the presence of all characteristic bands of pure Alg (Fig. 2B). Nevertheless, the presence of Gel resulted in a shift towards a higher wave number of the distinctive absorption bands of the carboxylate group of Alg at 1418.21 and 1618.80 cm – 1 to 1436.33 and 1638.07 cm – 1, respectively. The observed condition may be attributed to the electrostatic interactions that occur among the carboxyl compounds of Alg and the amino-acid compounds of Gel [36]. Notably, the amide I band at 1649.08 cm – 1 exhibited a noteworthy shift towards a lower wave number of 1638.07 cm-1, while the amide II band at 1546.97 cm – 1 displayed a shift towards a higher wave number of 1555.46 cm-1 with a concomitantly reduced intensity. These observations provide evidence for the participation of Gel's amide I and II in the Alg binding reactions [36].

Swelling rate

In tissue engineering, the swelling characteristic of applied biomaterials is a vital factor in achieving appropriate regenerative outcomes. The existence of swelling properties facilitates the interchange of nutrients, metabolites, and byproducts between the scaffolds and surrounding niches [37]. To be specific, swelling is a dynamic phenomenon and depends on mechanical deformation and mass transfer. These features are closely associated with the couplings between the carboxyl and hydroxyl moieties in the polymeric network backbone and water content [38].

In the present study, the swelling characteristics of Alg/Gel hydrogel were examined at 37 °C for 24, 48, 72, and 96 h (Fig. 2C). Data indicated an increase in the swelling ratio over time, with the maximum rate after 96 h. Of note, these values were 30.07, 60.85, and 79.39% for time points 24, 48, and 72 h, respectively.

It has been shown that Alg with anionic polysaccharides can easily absorb 200–300 folds of its weight after being incubated inside the aqueous phase [27]. In this regard, the immersion of Alg-based hydrogels in PBS facilitates an ion-exchange reaction between solution Na^+ ions and COO^- group-bound Ca^{2+} ions in the structure of the hydrogel [39]. Thus, the initiation of hydrogel swelling promotes the relaxation of the chain, followed by the electrostatic repulsion between negatively charged–COO^- groups. FT-IR analysis indicates that the addition of Gel into the Alg backbone correlates with reduced Ca^{2+} ion contents inside the Alg structure. This feature, in turn, can lead to the reduction of ionic strength, and cross-linked chains, enhancing elastic forces inside the Alg framework [40]. Overall, the reduction of the strength of ionic crosslinking can increase the hydrogel swelling rate, coinciding with water absorption [39]. Regarding the divalent entity of Ca^{2+} ions, it is postulated that this cation can generate a planar two-dimensional bonding. However, Ca^{2+} ions occupy the relatively smaller interstitial spaces within the Alg network, leading to the promotion of relaxation of the hydrogel. As expected, the ionic exchange and elimination of Ca^{2+} ions from the Alg structure can loosen the hydrogel stability [27]. Meanwhile, the existence of Gel in the structure's final composite increases the hydrophilic properties because of the intensity of the O-H stretching band, which per se heightens the reciprocal interaction between the water and hydrogel, leading to the reduction of hydrogen bonding within the hydrogel structure and thus enhancing the hydration properties [41].

Biodegradation rate

To this end, the degradation of Alg/Gel hydrogel was monitored for 12 days in the presence of lysozyme (Fig. 2D). Data showed an upward trend in the degradation rate of Alg/Gel hydrogel during the 12 days, in which the maximum effects were evident on day 12. A degradation rate of 9.51% was recorded after 2 days, and this rate reached approximately threefold (35.92%) on day 4. Based on the data, the biodegradation rate reached 66.13% after 12 days in in vitro conditions (Fig. 2D). An approximate two-fold increase in degradation rate after 4 days compared to a 2-day incubation period can be associated with the gradual release of Gel from Alg/Gel composite following swelling [42]. It is also postulated that the existence of ionic interaction can promote the replacement of Ca^{2+} ions with Na^+ ions, leading to hydrogel structure loosening and dissolution [27]. As mentioned above, the inclusion of Gel in the final composite acquires the hydrophilic characteristics within the polymeric network via the formation of hydrogel bonds. These features coincide with the inability of hydrogel to retain water in its structure [43]. Previous studies indicated that the degradation of Alg/Gel-based hydrogels is associated with two main factors as follows: discharge of Gel via diffusion and degradation, and inherent degradation of Alg structure [36]. It is suggested that the incorporated proteins can distribute within the hydrogel structure via pores, and easily discharge from the Alg backbone to the supporting aqueous phases. Even though the pore size and porosity of Alg hydrogel can, per se, affect the diffusion of Gel

[42]. Of note, the Gel molecules located on the surface of Alg/Gel hydrogels diffuse into the medium more quickly compared to molecules located in deep layers of hydrogels [36].

Mechanical properties

Porosity and pore size are fundamental regulators of mechanical performance with an inverse correlation [44]. Besides, chemical composition, crosslinking type and degree, along with the ionic strength of polymers, can influence the mechanical properties [45]. In the present study, the compressive stress-strain profile was measured at a constant stretched velocity of 2.0 mm min^{-1} to assess the effect of Gel on the mechanical behavior of Alg hydrogels. Additionally, the hydrogels' secant modulus of elasticity was calculated at 10% strain (Fig. 2E). Data indicated that hydrogel deformations were slightly enhanced with the increase in stress levels [46]. The Young's modulus was determined under a strain of 10%, and the inclusion of 1.125 wt% of Gel to Alg decreased dramatically Young's modulus of Alg hydrogel from 31 to 25 kPa. It was suggested that the viscoelastic characteristics of Alg become softer after the addition of Gel. Due to the reduced ionic strength between Alg and calcium, the cross-linking of Alg/Gel using Ca^{2+} ions exhibited the lowest possible values of G' and G". Besides, the presence of Gel in the final composite reduced the hydrogel's rigidity [27].

SEM imaging

SEM findings reveal that the encapsulated cells exhibited round to oval shape morphologies inside the Alg/Gel microspheres after 7 days (Fig. 3A). The internal space of Alg/Gel hydrogels was more prone to a fibrous and porous shape, and cells were appropriately entrapped within the Alg/Gel polymeric networks. Monitoring the external surface of Alg/Gel microspheres revealed several bulging cells, indicating the suitability of the Alg/

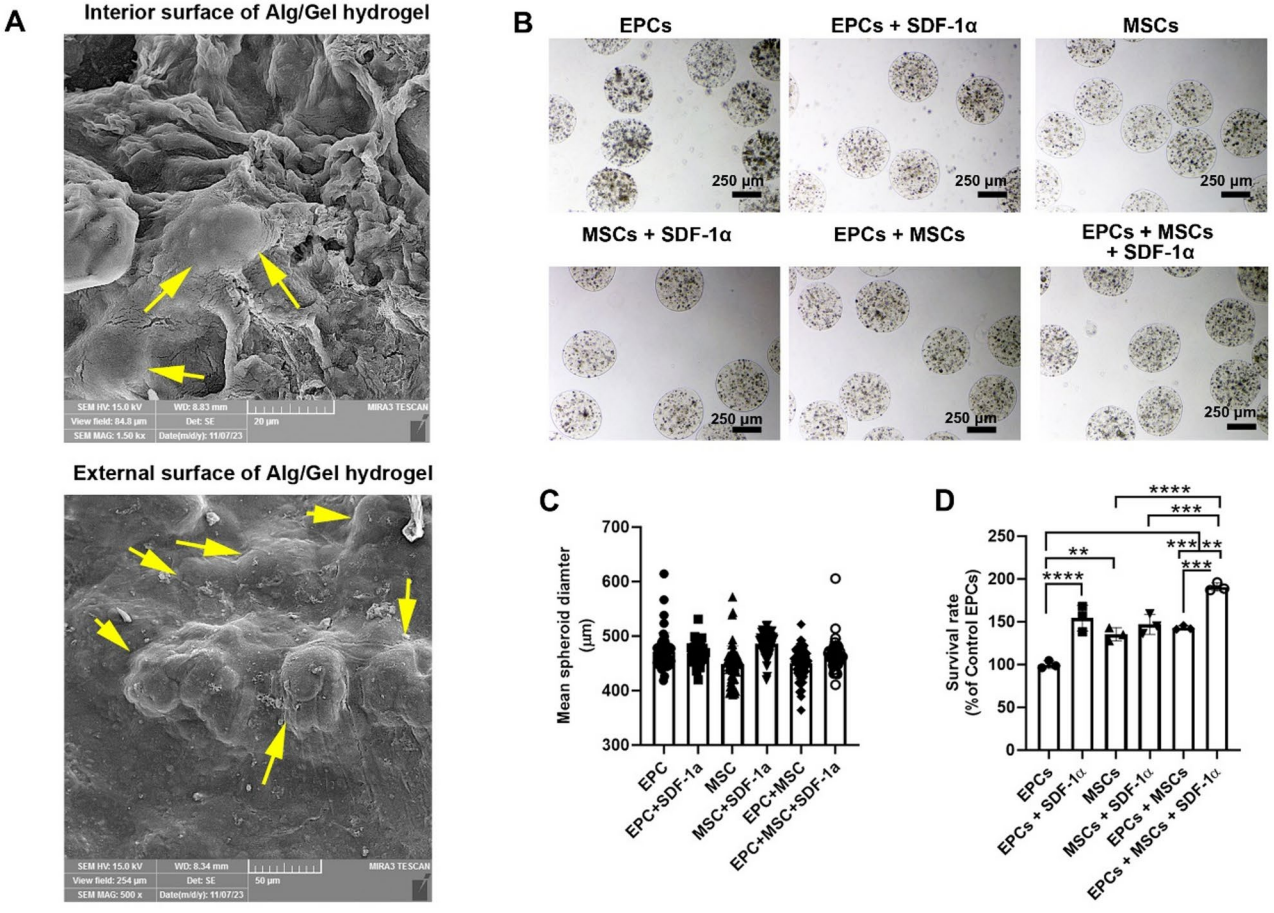

Fig. 3 SEM images (**A**). Upper panel: encapsulated cells can appropriately the polymeric network of Alg/Gel structure (yellow arrows). Lower panel: microsphere surface. Data show the bulging of cells from the external surface of Alg/Gel microspheres, indicating an appropriate cell localization and migration (yellow arrows). Bright-field images related to encapsulated EPCs and MSCs in the presence or absence of SDF-1α in side Alg/Gel microspheres after 7 days in in vitro conditions (**B**). Based on the data, cells were evenly distributed inside the microspheres. Non-significant differences were found in terms of microsphere diameter after 7 days ($n=50$). Measuring survival rate using MTT assay after 7 days ($n=3$). One-way ANOVA with Tukey post hoc analysis. $^{**}p<0.01$; $^{***}p<0.001$; $^{****}p<0.0001$

Gel polymeric network for cell motility and movement (Fig. 3A). These features indicated that Alg/Gel microspheres provide a suitable microenvironment for cell activity and morphological adaptation.

SDF-1α-loaded alg/gel hydrogel increased the survival rate

EPC-, MSC-, and EPC + MSC-loaded Alg/Gel microspheres enriched with 10 ng/ml SDF-1α were kept at culture conditions for 7 days (Fig. 3B). Bright-field images indicated that cell-laden microspheres exhibit discrete spherical particles containing evenly distributed cells with an average size of 464.33 ± 31.63 μm (Fig. 3B). Of note, a non-significant difference was found in terms of microsphere diameters in different groups after a 7-day culture period, indicating that the cells in the presence or absence of SDF-1α did not alter the microsphere diameters (Fig. 3C). The developed Alg/Gel microspheres had the potential to influence cell survival, in which the addition of 10 ng/ml SDF-1α increased the survival rate compared to SDF-1α-free groups ($P_{\text{EPCs vs. EPCs + SDF–1α}} < 0.0001$; $P_{\text{EPCs + MSCs vs. EPCs + MSCs + SDF–1α}} < 0.001$) (Fig. 3D). These changes were non-significant between the MSCs and MSCs + SDF-1α groups. Irrespective of SDF-1α addition, data indicated that cells can respond differently in terms of viability after being encapsulated inside Alg/Gel microspheres, in which statistically significant differences were found in the survival rate of MSCs and EPCs in the absence of SDF-1α. Interestingly, co-encapsulation of EPCs and MSCs can contribute to enhanced survival rates when compared to the single-cell encapsulated groups, and these features were intensified in the presence of SDF-1α. The addition of SDF-1α into the Alg/Gel microspheres increased the survival rate in EPCs + MSCs groups compared to matched control EPCs + MSCs microspheres (Fig. 3D).

SDF-1α-enriched alg/gel microspheres influenced angiogenesis and autophagy response

To monitor whether the encapsulation of EPCs and MSCs inside the SDF-1α-enriched Alg/Gel microspheres can alter the angiogenesis potential and autophagy response, western blotting analysis was done (Fig. 4). Protein lysate from three separate replicates was pooled, and protein levels of angiogenesis factors and autophagy-related factors (ATGs) were measured. Data indicated that protein levels of Ang-1 and Ang-2 were increased in groups with SDF-1α compared to matched control groups. Based on our data, the minimum Ang-1 and Ang-2 levels were detected in the MSCs groups, and the addition of SDF-1α increased Ang-1 and Ang-2, indicating the possible differentiation into vascular cells (Fig. 4). In EPCs, SDF-1α can increase both Ang-1 and Ang-2, resulting in improved angiogenesis potential. A similar pattern was achieved in the EPCs + MSCs + SDF-1α group compared to the EPCs + MSCs. According to our data, the addition of SDF-1α can lead to stimulation of Tie-2 in EPCs and EPCs + MSCs groups, while minor effects were achieved in MSCs. The increase of Tie-2

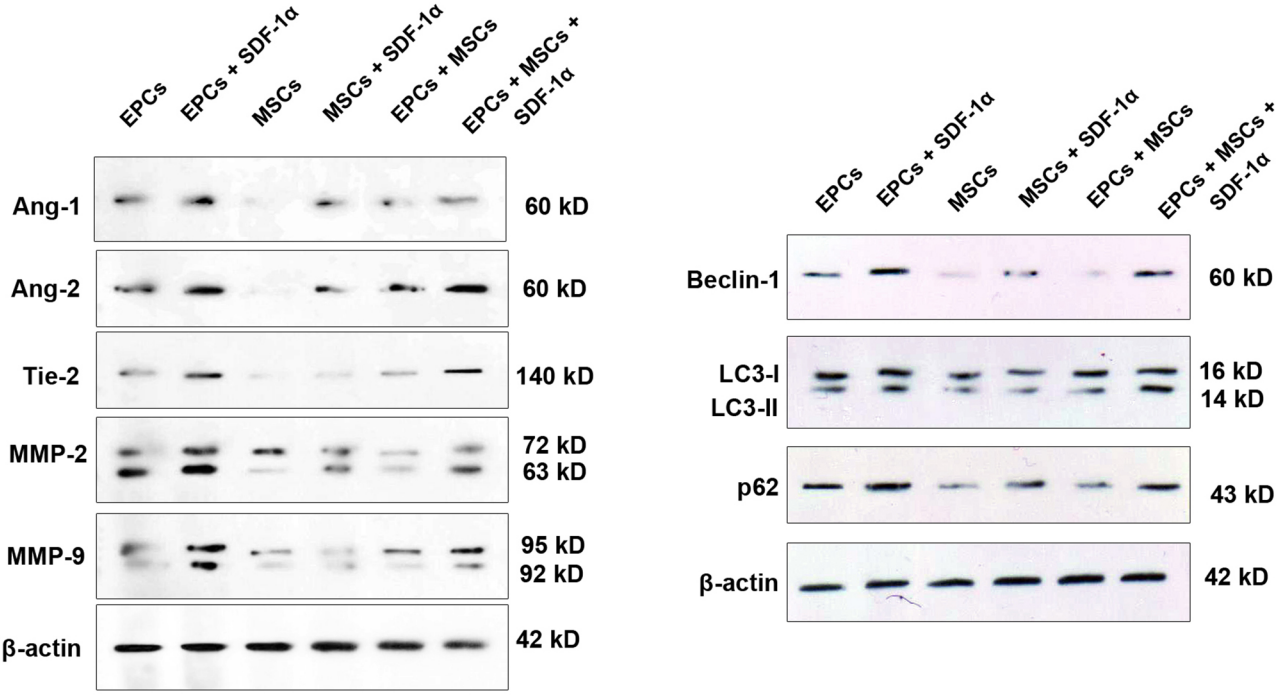

Fig. 4 Monitoring protein levels of angiogenesis (Ang-1, -2, and Tie-2), migration (MMP-2, and − 9), and autophagy factors (Beclin-1, LC3, p62) in encapsulated EPCs, MSCs inside the Alg/Gel microspheres with/without SDF-1α after 7 days. Data were obtained from three pooled samples

coincided with the stimulation of Ang-1 and Ang-2, indicating the activation of the angiogenesis axis, especially in EPCs, EPCs + MSCs groups in the presence of SDF-1α. The promotion of angiogenesis typically coincides with the migration of vascular cells to the target site [47]. Therefore, protein levels of matrix-degrading enzymes such as MMP-2 and − 9 were also measured. Data confirmed the prominent increase of total MMP-2 and − 9 in SDF-1α-enriched Alg-Gel microspheres containing EPCs, and EPCs + MSCs related to other groups. In the EPCs group, the levels of MMP-2 were more evident, while the levels of MMP-2 were less. Of note, encapsulated MSCs express low levels of both MMP-2 and − 9 when compared to the EPCs. These data indicated that encapsulated MSCs and EPCs inside the Alg/Gel microspheres are eligible to produce angiogenesis-related factors. Interestingly, particular stem cells, for example, EPCs, possess more angiogenesis properties, and the addition of certain growth factors such as SDF-1α can heighten this capacity. To find any possible relationship between the angiogenesis properties and autophagy status, protein levels of Beclin-1, LC3, and P-62 were also studied. In response to 10 ng/ml SDF-1α, encapsulated EPCs, MSCs, and EPCs + MSCs are prone to produce Beclin-1, an early-stage autophagic marker, compared to matched control SDF-1α-free groups after 7 days (Fig. 4). We found that EPCs containing groups, either EPCs or EPCs + MSCs encapsulated microspheres, produced higher levels of Beclin-1 compared to MSCs encapsulated groups. Again, in the presence of SDF-1α, total LC3 levels were higher in the encapsulated EPCs and EPCs + MSCs groups compared to the MSCs containing microspheres. In microspheres enriched with SDF-1a, the levels of LC3 were increased, indicating the promotion of autophagic flux, especially in EPCs containing microspheres. In the presence of SDF-1α, intracellular levels of P62 were also induced, and these effects were again more evident in EPCs containing microspheres compared to the MSCs group. These data indicate that the addition of SDF-1α into Alg/Gel microspheres can appropriately stimulate the autophagy response via the alteration of ATGs, especially in EPCs containing microspheres after 7 days.

SDF-1α-enriched alg/gel microspheres stimulated the in vitro tubulogenesis

The functionality of encapsulated EPCs and MSCs was evaluated using an in vitro tubulogenesis assay (Fig. 5A-B). For this purpose, encapsulated cells were released after 7 days from different experimental groups and plated on Matrigel-coated surfaces. The present data suggested that EPCs have higher tubulogenesis potential when plated on Matrigel substrates compared to MSCs. Based on our findings, the tubulogenesis properties of EPCs increased when these cells were pre-treated with 10 ng/ml SDF-1α within the Alg/Gel hydrogel microspheres ($P_{\text{EPCs Vs EPCs + SDF-1α}} < 0.0001$) (Fig. 5A-B). Notably, the plating of SDF-1α-free encapsulated MSCs did not result in the formation of tube-like structures, and only small-sized cell microaggregates were evident on the surface of Matrigel. The encapsulation of MSCs inside Alg/Gel hydrogel in the presence of SDF-1α was shown to relatively improve the tubulogenesis properties; however, this property is still less when compared to the EPC + SDF-1α group ($p < 0.0001$) (Fig. 5A-B). Despite the existence of minimal tube-like structures in the MSCs + EPCs group, the addition of SDF-1α can, in part, improve tubulogenesis capacity similar to the MSCs + SDF-1α and EPCs groups. In general, these data show that encapsulation of EPCs within the Alg/Gel microspheres, along with SDF-1α, can significantly increase in vitro angiogenesis properties. However, these features were not statistically significant as compared to matched control SDF-1α-free groups.

Migration of encapsulated cells was stimulated in the presence of SDF-1α

Transwell insert migration assay indicated that the number of encapsulated cells that passed the pores was stimulated pre-treated with SDF-1α, in which statistically significant differences were observed in terms of migrated cells in groups EPCs, MSCs, and EPCs plus EPCs in comparison with SDF-1α-free groups (Fig. 5C). Interestingly, the juxtaposition of MSCs and EPCs inside the Alg/Gel microspheres in the absence of SDF-1α can improve the migration capacity when compared to encapsulated EPCs but not the MSCs group (Fig. 5C). These features indicate the possible synergetic properties of EPCs and MSCs to stimulate migration properties. Along with the obtained data, it can be said that the encapsulation of EPCs and MSCs in SDF-1α-bearing Alg/Gel microspheres can influence the migration properties of these cells in the in vitro Matrigel tubulogenesis assay.

Angiogenesis array

Using an angiogenesis array, the expression of multiple genes was monitored in cultured EPCs, MSCs, and EPCs + MSCs within the Alg/Gel microspheres in the presence and/or absence of SDF-1α (Table 2; Fig. 5D). Based on the obtained data, co-incubation of EPCs with SDF-1α can increase the expression of PECAM1 (CD31; ~125.37-fold), indicating the maturation of isolated EPCs toward the mature endothelial cells (ECs). It seems that in the presence of SDF-1α, MSCs can also express CD31 levels. These features were moderate in EPCs + MSCs and EPCs + MSCs + SDF-1α groups. The expression of ERBB2, a HER2 receptor tyrosine kinase, was up-regulated in EPCs + SDF-1α, while the juxtaposition of EPCs with MSCs within the Alg/Gel microspheres

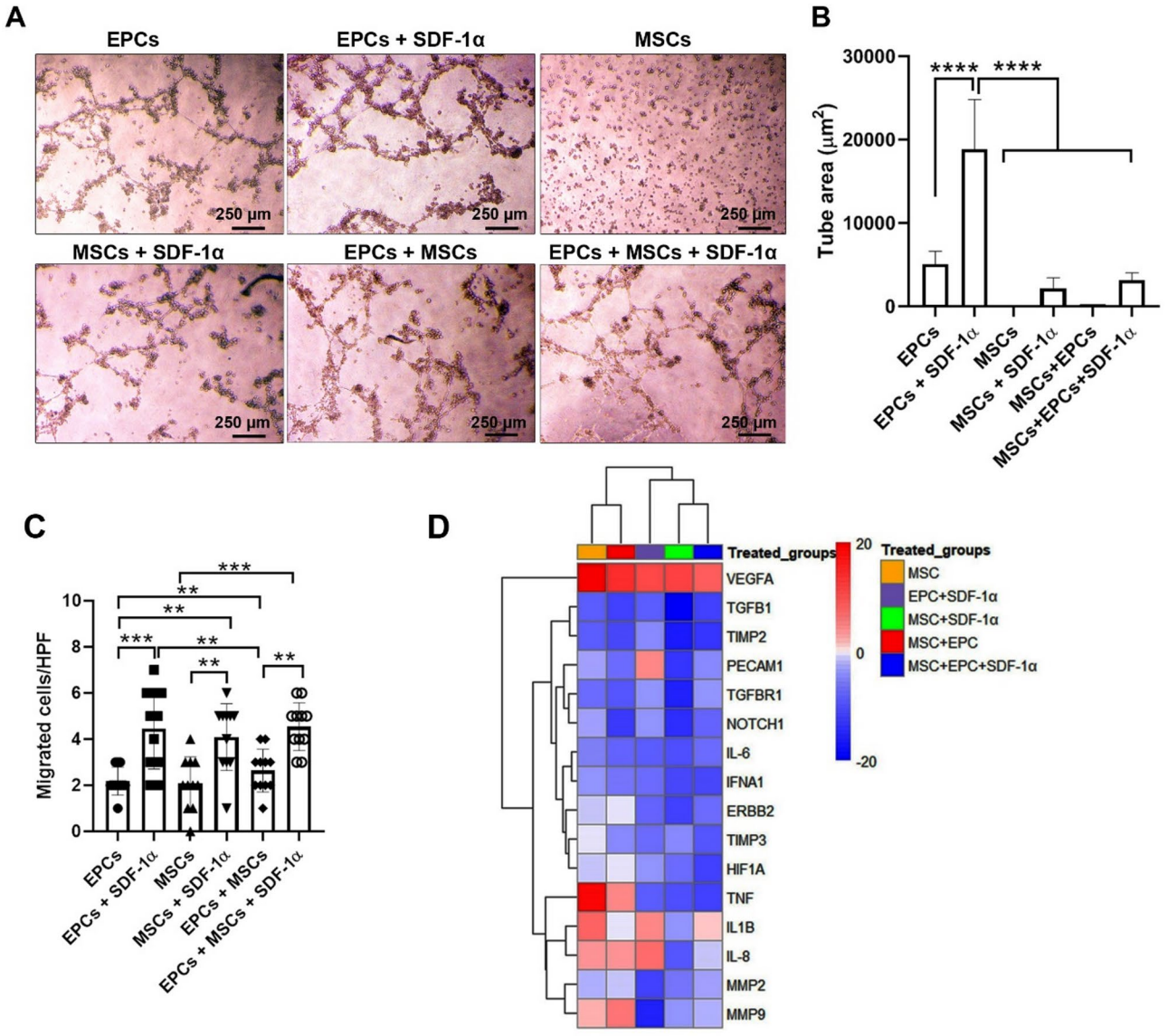

Fig. 5 Monitoring the tubulogenesis properties of EPCs, MSCs pre-cultured inside Alg/Gel microspheres after 7 days (**A-B**; $n=3$). The migration rate was monitored using the Transwell insert system (**C**; $n=11$). PCR array analysis for the detection of angiogenesis profile (**D**; $n=3$). Fold-changes greater than 2 are indicated in red; fold-changes less than −2 are indicated in blue. One-way ANOVA with Tukey post hoc analysis. $^{**}p<0.01$; $^{***}p<0.001$; $^{****}p<0.0001$

yielded 29.45-fold expression. It seems that the type of microspheres can appropriately increase the expression of ERBB2 in MSCs as well. It was shown that the levels of pro-inflammatory cytokines such as IL-1β, IL-6, and IL-8 were also increased in different experimental groups, but these values were more evident in terms of IL-8 (Table 2; Fig. 5D). Of note, the expression of HIF-1α coincides with the co-upregulation of VEGF in different groups, especially in MSCs and EPCs + MSCs groups. Along with these changes, the expression of NOTCH1 was also induced in MSCs, EPCs + SDF-1α, and MSCs + EPCs + SDF-1α (Table 2; Fig. 5D). These features show that the encapsulation of EPCs, MSCs, and their combination inside the Alg/Gel microspheres can alter the expression of various genes related to angiogenesis properties.

Histological examination

H & E and masson's trichrome staining

In the current study, experimental acute myocardial infarction was induced using LAD ligation in rabbits (Fig. 6A). Data indicated a significant reduction of infarct zone in all groups that received cells compared to the control infarct rabbits (Fig. 6B). Data from Masson's trichrome staining indicated that the injection of cells from the EPCs + SDF-1α group did not yield statistically significant differences compared to the EPCs group, indicating that the incorporation of SDF-1α cannot

Table 2 Angiogenesis array of encapsulated epcs, mscs, EPCs + MSCs within alg/gel microspheres in the presence or absence of SDF-1α

Gene	Fold change compared to the control EPCs group				
	EPCs + SDF-1	MSCs	MSCs + SDF-1α	EPCs + MSCs	MSCs + EPCs + SDF-1α
PECAM1	125.37	13.04	0.41	3.16	8.43
ERBB2	3.10	23.83	0.71	29.45	3.54
IL1B	143.01	331.99	10.23	25.99	53.63
TGFB1	1.96	2.12	0.05	0.74	0.70
IL-6	1.99	6.43	1.14	2.83	3.33
TGFBR1	10.06	3.99	0.19	1.71	10.52
IL-8	282.09	105.79	1.48	106.15	23.51
TIMP2	7.57	2.15	0.16	0.99	0.40
TIMP3	3.48	28.54	6.94	7.78	1.75
HIF1A	10.63	19.49	3.40	30.27	0.75
MMP2	0.76	16.17	5.08	21.86	12.68
IFNA1	3.89	8.85	0.93	4.06	1.06
MMP9	0.22	68.83	11.12	210.84	14.98
VEGFA	942.27	20666.41	1230.48	2702.35	447.27
TNF	2.04	15024.19	1.14	118.60	0.77
NOTCH1	10.70	13.41	0.35	0.59	2.90

Fold-changes greater than 2 are indicated in red; fold-changes less than −2 are indicated in blue ($n = 3$)

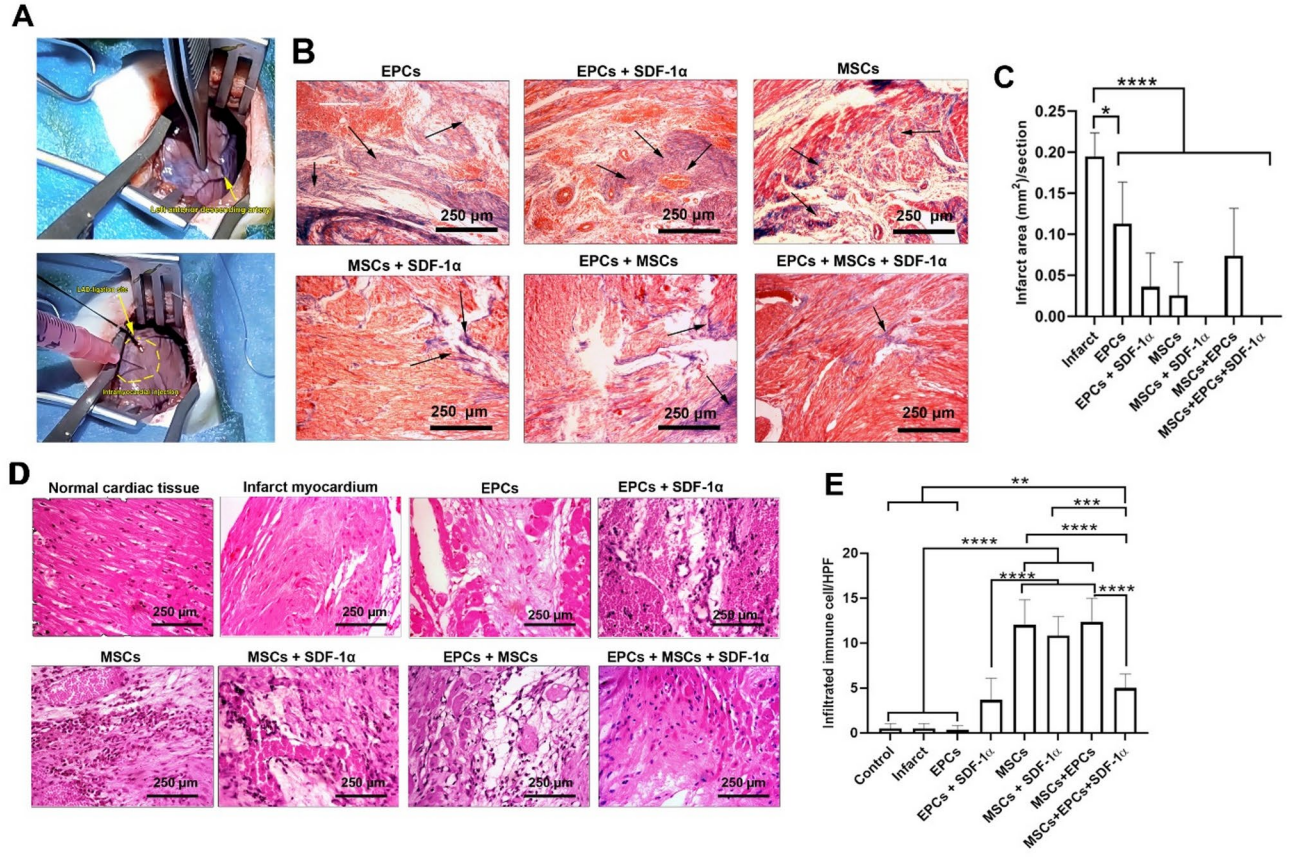

Fig. 6 Induction of MI in rabbits using LAD ligation (**A**). Cells were administered into the border zone of ischemic sites (yellow arrows and dashed circular area). Histological analysis revealed the existence of blue-colored collagen fibers in different groups (**B**; black arrows). Measuring the fibrotic area per cardiac tissue slide using Masson's trichome staining (**C**; $n = 6$). H & E staining (**D**). Number of immune cells infiltrated into the periphery of the ischemic zone in MI rabbits (**E**; $n = 6$). One-way ANOVA with Tukey post hoc analysis. *$p < 0.05$; **$p < 0.01$; ***$p < 0.001$; and ****$p < 0.0001$

increase the antifibrotic properties of EPCs. According to the obtained data, rabbits in the MSCs + SDF-1α and MSCs + EPCs + SDF-1α groups exhibited the minimum scar tissue in the myocardium compared to other groups. MSCs, either alone or in combination with EPCs, can efficiently diminish myocardial fibrosis when pre-treated with SDF-1α (Fig. 6B-C). H & E staining showed dense fibrosis in the infarcted myocardium. Similar to Masson's trichrome staining, in the EPCs group, the density and extent of fibrotic area were reduced. In rabbits that received the combination of EPCs + SDF-1α, myocardial hyperemia adjacent to distributed inflammatory cells can be detected. In the MSCs group, numerous recruited immune cells, mostly mononuclear cells, infiltrated the interstitial space of cardiac tissues, while in the MSCs + SDF-1α local hyperemia with reduced immune cell numbers is evident. In the EPCs + MSCs group, slight hyperemia was evident, and the number of recruited immune cells diminished in the borderline (Fig. 6D-E). Based on our calculation, no significant differences were found in terms of infiltrated immune cells in EPCs and infarct groups when compared to the control rabbits ($p > 0.05$; Fig. 6E). The largest number of infiltrated immune cells was found in MSCs, MSCs + SDF-1α, and EPCs + MSCs groups compared to the Control, Infarct, and EPCs groups ($p < 0.05$). Notably, the number of immune cells was lower in the EPCs + SDF-1α group compared to the MSCs, MSCs + SDF-1α, and EPCs + MSCs groups ($p < 0.05$). Data indicated the existence of cardiomyocyte-like cells in the border zone of the ischemic myocardium that received EPCs + MSCs + SDF-1α without active immune system response, and local hyperemia. Commensurate with these data, it can be said that injection of MSCs and EPCs pre-treated with SDF-1α within the Alg/Gel hydrogel can improve the healing process of ischemic myocardium after 30 days compared to single-cell injection, either EPCs or MSCs with or without SDF-1α.

SDF-1α stimulated the angiogenesis properties of stem cells in ischemic myocardium

The in vivo angiogenesis potential of encapsulated EPCs and MSCs in the presence and/or absence of SDF-1α was monitored using IHC staining of α-SMA$^+$ and CD31$^+$ vessels after 30 days (Fig. 7). Data indicated that the direct injection of EPCs with SDF-1α pre-treatment inside the Alg/Gel microspheres led to a significant increase of α-SMA$^+$ arterioles in ischemic myocardium when compared to the other experimental groups ($p < 0.05$; Fig. 7A). We noted that co-incubation of EPCs with SDF-1α inside the Alg/Gel microspheres for 7 days stimulated the arteriogenesis capacity of these cells when compared to the EPCs groups. Of note, non-significant differences were found in terms of α-SMA$^+$ arterioles in EPCs when compared to the MSCs group. Either in MSCs and MSCs + SDF-1α groups, the lowest vascular densities when obtained compared to other groups ($p < 0.05$; Fig. 7A). However, co-administration of EPCs and MSCs pre-encapsulated inside the Alg/Gel microspheres with/without SDF-1α led to higher arteriogenesis properties compared to the MSCs and MSCs + SDF-1α groups. No statistically significant differences were obtained between the EPCs + MSCs and EPCs + MSCs + SDF-1α groups ($p > 0.05$). These data showed the superior arteriogenesis potential of EPCs when maintained inside the Alg-based hydrogels with SDF-1α or co-administration with MSCs in the rabbit model of MI. According to the present data, higher microvascular (CD31$^+$ vessels) were found in rabbits that received EPCs and/or EPCs + SDF-1α compared to the other experimental groups ($p < 0.05$; Fig. 7B). Although in EPCs + MSCs and EPCs + MSCs + SDF-1α groups, the local density of CD31$^+$ capillaries increased compared to the MSCs and MSCs + SDF-1α groups, these differences did not reach statistically significant levels. These data revealed the significant arteriogenesis and angiogenesis capacities of EPCs in the presence or absence of SDF-1α inside the Alg/Gel hydrogel for 7 days before injection into the ischemic myocardium.

Discussion

The current study deals with the reparative properties of encapsulated EPCs, MSCs, and their combination inside Alg/Gel microspheres in the presence of SDF-1α for the induction of vascularization in a rabbit model of MI. According to the present data, the suitable physicochemical properties of the Alg/Gel polymeric network induced by $CaCl_2$ for regenerative purposes. SEM results indicated that encapsulated cells favorably attached to the Alg/Gel network and acquired flattened morphologies. Suitable attachment of stem cells with a polymeric network consisting of Alg-based hydrogels has been reported and is an essential item for regulating cell survival, proliferation, and differentiation properties [48]. The addition of Gel to the final composites can aid the encapsulated cells, like EPCs and MSCs, to directly interact with various Gel motifs such as RGD and RGDS via engaging membrane-bound integrins with [49, 50]. In this regard, this platform supports cell survival and suitable motility inside the Alg/Gel microspheres, in which on the external surface of the microspheres, bulging cells are detected in the SEM images. Because of biocompatibility and suitable surface features, the encapsulated cells are evenly distributed inside the Alg/Gel microspheres, as evident in bright-field images. It was suggested that 7-day incubation of EPCs alone and in combination with MSCs with 10 ng/ml SDF-1α can significantly stimulate the survival rate compared to matched control SDF-1α-free and MSCs, MSCs + SDF-1α groups. SDF-1α can stimulate the

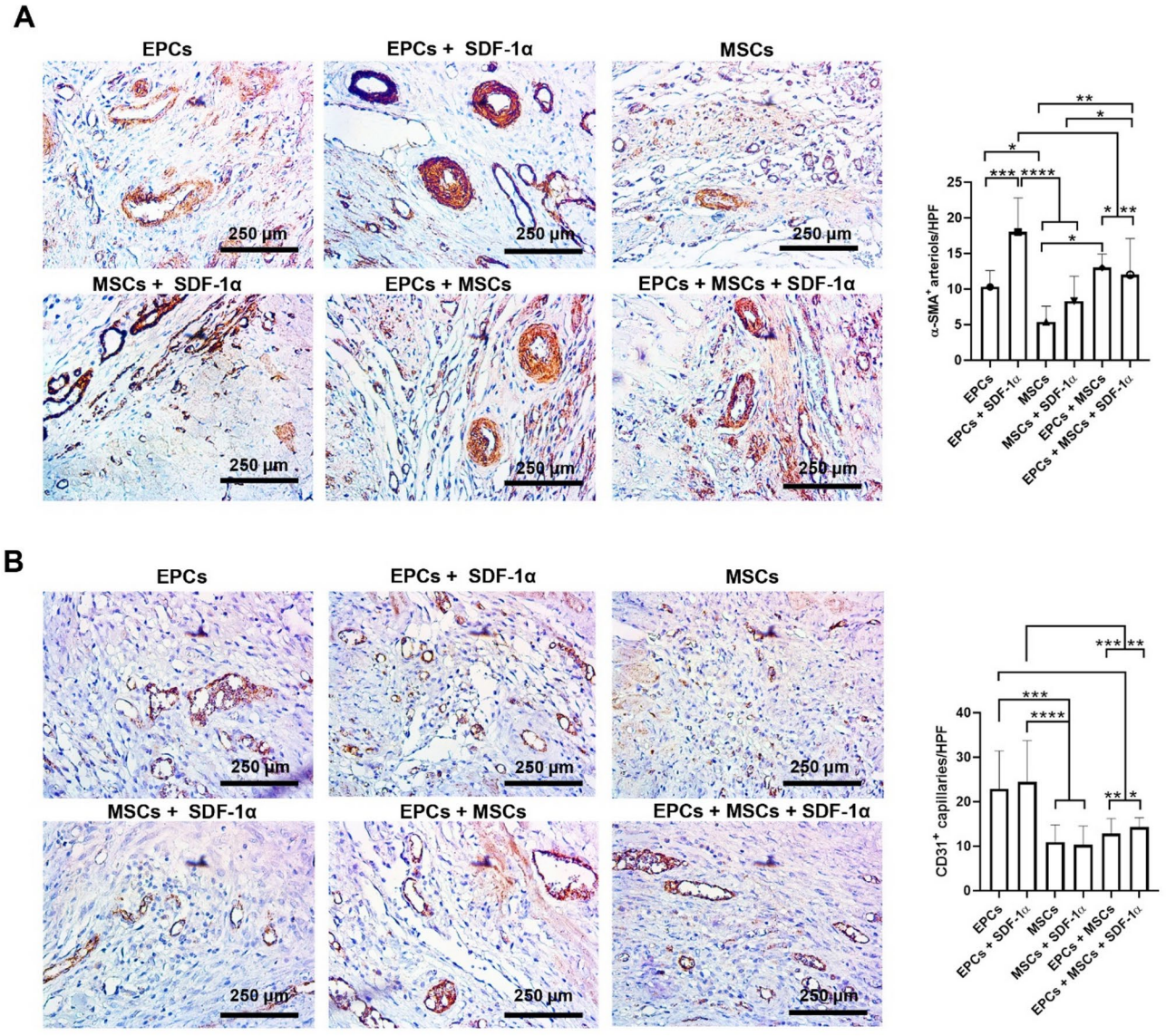

Fig. 7 Monitoring the arteriogenesis and angiogenesis properties of EPCs and MSCs pre-cultured inside the Alg/Gel microspheres for 7 days in the presence and absence of SDF-1α in MI rabbits after 30 days (**A**-**B**). Local density of α-SMA$^+$ arterioles (**A**) and CD31$^+$ capillaries (**B**). One-Way ANOVA with Tukey post hoc. ($n=6$ rabbits per group, and data were obtained from 10 serial HPF). *$p<0.05$; **$p<0.01$; ***$p<0.001$; and ****$p<0.0001$

proliferation and commitment of stem cells toward target lineage via the alteration of various signaling pathways [51]. Cun and co-workers indicated the enhanced proliferation capacity of EPCs by the SDF-1/CXCR4 signaling pathway in an ERK/Akt-dependent manner [52]. Based on our data, co-encapsulation of EPCs and MSCs inside the SDF-1α-bearing Alg/Gel microspheres intensified the survival effects compared to matched control encapsulated single-cell groups. This feature can be related to the synergistic effects of MSCs and EPCs in terms of survival rate and angiogenesis potential. For example, it was shown that co-culture of MSCs with EPCs led to the increase of local VEGF contents, and functional maturity of EPCs indicated by enhanced AC-LDL uptake, and maturation into CD31$^+$, and vWF$^+$ vascular cells [53, 54]. Interestingly, we did not find any statistically significant differences in terms of viability between MSCs and MSCs + SDF-1α in the presence of SDF-1α. However, MSCs exhibited a higher survival rate compared to EPCs in SDF-1α-free microspheres. These data would be from the fact that MSCs may possess broad adaptation properties compared to other stem cell types. Previous data have indicated inherently different doubling times and proliferation capacities between stem cells from various tissues [55]. Whether MSCs and EPCs can respond differently to the Alg/Gel microspheres needs further investigation.

Proteomic analysis revealed the induction of angiogenesis properties in encapsulated cells within the Alg/Gel microspheres containing 10 ng/ml SDF-1α. The levels of Ang-1, -2, and Tie-2 were prominently increased in EPCs + SDF-1α and EPCs + MSCs + SDF-1α groups, with less effect in MSCs containing microspheres. Genomic data also indicated the promotion of angiogenesis signaling pathways by engaging different effectors. The high expression of VEGF and HIF-1α in MSCs containing microspheres showed that these cells tend to manage the angiogenesis phenomenon possibly in paracrine manner via the secretion of different factors instead of direct differentiation into the mature ECs [56] while the expression of Ang-1, Ang-2, Tie-2, Notch1, and (PECAM1) CD31 in EPCs-loaded microspheres indicate the promoted maturation of EPCs toward functional ECs. However, the possibility of vascularization via the production of angiocrine should not be excluded in EPCs-loaded microspheres. In support of this claim, the transcription rate of PECAM1 was higher in EPCs-bearing groups compared to MSCs groups. Although the existence of SDF-1α can increase the possibility of endothelial differentiation via the expression of PECAM1. Consistent with PCR array and western blot data, microvascular density, either $CD31^+$ capillaries or α-SMA^+ arterioles, was induced in EPCs and EPCs + SDF-1α groups compared to MI rabbits that received MSCs, or SDF-1α-treated MSCs. An intermediate state was observed in the MSCs + EPCs and MSCs + EPCs + SDF-1α groups. Taken together, these data confirmed the higher differentiation and maturation capacity of EPCs versus MSCs in the generation of ECs. The expression of IL-8 is different in experimental groups, especially EPCs + SDF-1α, indicating the promotion of EC dynamic growth, survival, and migration in the encapsulated cells [57]. It has been shown that the changes in MMPs can also be related to the activation of IL-8 during the pro-angiogenesis signaling pathway. Some documents have revealed the close relationship between IL-8 and SDF-1α, in which the low concentrations of SDF-1α can increase the local density of IL-8, MCP-1, and other cytokines [58]. Of note, the role of IL-8 in fibrosis and regeneration is context-dependent and depends on the type and intensity of pathologies [59]. It seems that the simultaneous increase of other angiogenesis factors led to the promotion of angiogenesis effects rather than the fibrotic properties. The close relationship between the autophagy status and angiogenesis potential of encapsulated EPCs, MSCs, and their combination was also monitored in response to SDF-1α. Data indicated that SDF-1α can stimulate the autophagy response (Beclin-1↑, total LC3↑) in encapsulated EPCs, MSCs, and EPCs + MSCs compared to matched control SDF-1α-free groups. Previously, Herberg et al. declared that SDF-1β-expressing bone marrow MSCs can activate the autophagic response (Beclin-1↑and LC3B-II/-I ratio↑) when exposed to H_2O_2, leading to reduction of apoptotic changes (Cleaved Caspase-3↓, and PARP↓) in harsh microenvironments [60]. It has been shown that SDF-1α can increase the autophagic flux (autophagosomes↑ and autolysosomes↑) in chondrocytes via the up-regulation of ULK-1, LC3B, and Beclin-1 in a CXCR4/mTOR signaling axis-dependent manner [61]. Further activation of AMPK by SDF-1α reduces NLRP3 inflammasome formation, and pyroptosis (GSDMD↓ and IL-1β↓, Caspase-1↓) in human synoviocytes, indicating that the close interaction of SDF-1α with autophagy signaling cascade (AMPK/PI3K/mTOR axis) controls the survival rate [62]. Although the increase of intracellular p62 is integral to incomplete autophagy response [63], higher levels of this factor contribute to protection against oxidative stress and inflammation via the activation of Nrf-2 and Keap1 [64]. Considering the data from the MTT panel and enhanced survival rate in SDF-1α-treated groups, it seems that the increase of intracellular p62 levels is not to the extent that it exerts toxic effects. Irrespective of the direct SDF-1α effect on the angiogenesis potential of encapsulated EPCs, MSCs, and EPCs + MSCs within the Alg/Gel microspheres, whether and how autophagy modulation can affect the process of vascularization or vice versa is at the center of debate. Recent data have indicated the close relationship between angiogenesis-related factors and autophagy machinery. For example, the injection of Ang-2 in rabbits with radius bone defects that received hydroxyapatite/collagen scaffold led to the increase of $CD31^+$ capillaries and local elevation of VEGF at the site of injury [65]. Along with these changes, autophagic proteins such as Beclin-1, LC3-II/-I ratio, and p62 are also stimulated [65]. In our previous study, we found that treatment of $CD146^+$ stem cell-derived ECs with Met led to the increase of VE-cadherin and vWF, resulting in angiogenesis potential [66]. Notably, in the $tie^{-/-}$ knockout mouse macrophages, the reduced levels of VEGF, the LC3-II/-I ratio led to the suppression of choroidal neovascularization after laser irradiation [67]. Therefore, it can be pointed out that the reciprocal interaction between angiogenesis and autophagy in the presence of SDF-1α can intensify the potency of *de novo* blood vessel formation in EPCs and MSCs. In vitro tubulogenesis assay also indicated the superior angiogenesis properties in encapsulated cells that received SDF-1α, and this property reached the maximum levels in the EPCs + SDF-1α group. One reason for the alignment and juxtaposition of cells to form tube-like structures is that the stimulation of the CXCR-4 signaling axis via SDF-1α can lead to the sustained expression of VE-cadherin [68]. This factor is thought to be involved in EC-to-EC connection and the formation of the endothelial barrier [69]. The alignment and localization of vascular cells are

closely dependent on the migration capacity, and these properties were shown to be significantly stimulated in the presence of SDF-1α in EPCs + SDF-1α, MSCs + SDF-1α, and EPCs + MSCs + SDF-1α groups. According to our data, the cardiac fibrotic area was significantly diminished in rabbits that received EPCs, MSCs, and EPCs plus MSCs compared to the control infarct animals. The reduction of myocardial fibrosis is in part related to enhanced angiogenesis potential and inhibition of fibrosis-related effectors [70]. These effects were more evident in MSCs containing groups pre-treated with SDF-1α. It has been indicated that transplanted MSCs can regulate the progression of fibrosis within the ischemic myocardium via different mechanisms. For instance, MSCs are putative progenitors to reduce the conversion of cardiac fibroblasts to myofibroblasts, increase the MMP levels, and diminish the aberrant remodeling via reduced collagen deposits [71]. While commitment into cardiomyocyte-like cells can prohibit the expansion of myocardial fibrosis [72]. Data from the angiocrine panel also confirms the up-regulation of MMP-2 and −9 in the presence of SDF-1α. However, it seems that co-administration of EPCs with MSCs can efficiently reduce collagen deposition in the border zone of ischemic myocardium. It seems that SDF-1α treatment can also increase the paracrine activity of stem cells to recruit immune cells into the ischemic area, evident in H & E slides [73]. The lack of a similar pattern in gene expression and protein levels of MMP-2 and −9 analyzed by western blotting and PCR array analysis can be related to several parameters. For instance, it was suggested that post-transcriptional modifications, the control of translation, and peptide/protein stability and activity are important [74]. Previous data have indicated that the specific types of MMPs exhibit different degrees of stability [75]. Besides, activation of some factors, such as TGF-β, is integral to MMP expression and half-life. TGF-β can increase the expression of MMP-2 and −9 via the SMAD signaling pathway [76]. Despite the critical role of MMPs in the function and regenerative medicine of both MSCs and EPCs. It is also possible that different activation and releasing systems are used by EPCs and MSCs. MSCs can produce and release high levels of TIMPs, which can regulate the subcellular localization and activity of MMPs [77]. In contrast, EPCs have higher MMP activity due to their direct role in the stimulation of vascularization [78].

The current study faces some limitations and weaknesses that need further investigation for deeper analyses. Although it cannot be generalized to all cases, labeling and tracking the cells after being transplanted into the border zone of MI rabbits and other MI models can help us in the determination of their bioactivities and accurate regenerative potential [79]. This strategy enables to monitoring of the in-situ differentiation and/or migration of transplanted cells. Using various survival analyses, it is possible to monitor the number of living cells at the site of injection, indicating the cell-based therapy outcomes [31]. Although several studies have indicated the immunomodulatory properties of both human EPCs and MSCs in xenogeneic animal models [80, 81], it is recommended to use allogenic and/or autologous EPCs and MSCs rather than xenogeneic cell sources to reduce or eliminate the inflammation and thus transplant rejection.

Conclusion

The promotion of angiogenesis and *de novo* blood vessel formation is thought of as an efficient therapeutic strategy in the acceleration of tissue healing in MI candidates. Due to the existence of a harsh microenvironment and stressful conditions, large fractions of transplanted cells undergo atrophic changes and lack an appropriate regenerative outcome. Here, it was indicated that the culture of EPCs and MSCs inside the Alg/Gel microspheres enriched with SDF-1α before transplantation can improve the reparative parameters of these cells. Based on the obtained data, the EPCs prefer to alleviate the ischemic myocardium mainly via maturation into the ECs, while MSCs activate the angiocrine activity to promote the angiogenesis properties. The current study highlighted the supportive impacts of Alg/Gel microspheres to not only preserve the angiogenesis properties of EPCs and MSCs but also increase their bioactivities after being injected into the ischemic myocardium. Further studies should focus on the determination of diverse signaling pathways involved in the angiogenesis properties of EPCs and MSCs pre-cultured in 3D niches before administration into the ischemic areas.

Abbreviations

Alg/Gel	Alginate/Gelatin
ATGs	Autophagy-related factors
BM	Bone marrow
BSA	Bovine serum albumin
CABG	Coronary artery bypass grafting
Dil-Ac-LDL	Dil-labeled Acetylated low density lipoprotein
ECs	Endothelial cells
EPCs	Endothelial progenitor cells
ECM	Extracellular matrix
FBS	Fetal bovine serum
HPF	High-power fields
IHC	Immunohistochemistry
IHD	Ischemic heart disease
LAD	Left anterior descending coronary artery
LV	Left ventricles
MMPs	Matrix metalloproteinases
MSCs	Mesenchymal stem cells
MCP-1	Monocyte chemoattractant protein-1
MNCs	Mononuclear cells
MI	Myocardial infarction
SEM	Scanning electron microscope
SDF-1α	and Stromal cell-derived factor 1 alpha
TIMPs	Tissue inhibitors of metalloproteinases

Supplementary Information

The online version contains supplementary material available at https://doi.org/10.1186/s12964-025-02301-0.

Supplementary Material 1
Supplementary Material 1
Supplementary Material 2
Supplementary Material 2
Supplementary Material 3
Supplementary Material 3
Supplementary Material 4
Supplementary Material 4
Supplementary Material 5
Supplementary Material 5
Supplementary Material 6
Supplementary Material 6
Supplementary Material 7
Supplementary Material 7
Supplementary Material 8
Supplementary Material 8
Supplementary Material 9
Supplementary Material 9
Supplementary Material 10
Supplementary Material 10

Acknowledgements
Authors would like to thank the personnel of the Faculty of Advanced Medical Sciences, and Stem Cell Research Center of Tabriz University of Medical Sciences, and the Faculty of Veterinary (affiliated with the University of Tabriz) for guidance and help in the progression of this project. The authors declare that they have not used Artificial Intelligence in this study.

Author contributions
H.A., Ç.B.A., S.N.K., A.H., M.A., N.M., S.S., M.T.N., L.S.T., M.S. T., M. N., S.H. performed different analyses and prepared the draft. A.B.K. and R.R. acquired funding, supervised the study, and edited the final manuscript.

Funding
This study originated from a clinician scientist's Ph.D. thesis. Research reported in this publication was supported by the Elite Researcher Grant Committee under award number [IR.NIMAD.REC.1400.151] from the National Institute for Medical Research Development (NIMAD), Tehran, Iran, and Tabriz University of Medical Sciences under the ethical code of IR.TBZMED.REC.1399.125.

Data availability
Data will be available on resealable request.

Declarations

Ethics approval and consent to participate
In this study, the informed consent process was done by the children's parents without any interference in the diagnosis process and therapeutic protocols, and samples were prepared according to the Declaration of Helsinki (1964). The current study was conducted according to the previously published guidelines and was registered as titled "Angiogenic properties of mesenchymal stem cells and endothelial progenitor cells encapsulated inside alginate microspheres in a rabbit model of myocardial infarction" under an approval code of IR.TBZMED.REC.1399.125 from Research Ethics Committees of Vice-Chancellor in Research Affairs - Tabriz University of Medical Sciences on 2020-05-04, and by the Elite Researcher Grant Committee under award number [IR.NIMAD.REC.1400.151] from the National Institute for Medical Research Development (NIMAD), Tehran, Iran on 2021-11-30.

Consent for publication
Not applicable.

Competing interests
The authors declare no competing interests.

Author details
[1]Stem Cell Research Center, Tabriz University of Medical Sciences, Imam Reza St., Golgasht St, Tabriz, Iran
[2]Department of General and Vascular Surgery, Tabriz University of Medical Sciences, Tabriz, Iran
[3]Department of Medical Biology, Faculty of Medicine, Ege University, Izmir, Turkey
[4]Chemical Engineering Faculty, Sahand University of Technology, Tabriz 51335- 1996, Iran
[5]Student Research Committee, Tabriz University of Medical Sciences, Tabriz, Iran
[6]Department of Applied Cell Sciences, Faculty of Advanced Medical Sciences, Tabriz University of Medical Sciences, Tabriz, Iran

Received: 10 March 2025 / Accepted: 8 June 2025
Published online: 12 June 2025

References

1. Yesmin S, et al. Knowledge regarding myocardial infarction (MI) among the nurses in dhaka, Bangladesh. Int J Sci Bus. 2022;14(1):108–15.
2. Seslier T, Karakuş MÖ. In healthcare applications of machine learning algorithms for prediction of heart attacks. J Sci Reports-A (051):358–70.
3. Gaudel P. Effects of intervention on lifestyle changes among coronary artery disease patients: A 6-month follow-up study A Randomized Controlled Trial. 2022;9(4):2024–2036. https://doi.org/10.1002/nop2.1212
4. Jafari Sorkhdehi MM et al. Decellularization and characterization of camel pericardium as a new scaffold for tissue engineering and regenerative medicine. Asian Cardiovasc Thorac Ann. 2024 May;32(4):194–199.
5. Amini H et al. Exosome-bearing hydrogels and cardiac tissue regeneration. Biomaterials Res. 27(1):99.
6. Wang S, et al. Exosomes derived from TNF-α-treated bone marrow mesenchymal stem cells ameliorate myocardial infarction injury in mice. Organogenesis. 2024;20(1):2356341.
7. Raleigh MJ, et al. Endothelial progenitor cells for diabetic cardiac and kidney disease. Stem Cells Transl Med. 2024;13(7):625–636.
8. Yu H, et al. Stem cell therapy for ischemic heart diseases. Br Med Bull. 2017;121(1):135–54.
9. Huang H, Huang W. Regulation of endothelial progenitor cell functions in ischemic heart disease: new therapeutic targets for cardiac remodeling and repair. Front Cardiovasc Med. 2022;9:896782. https://doi.org/10.3389/fcvm.2022.896782
10. Yan F, et al. Paracrine mechanisms of endothelial progenitor cells in vascular repair. Acta Histochem. 2022;124(1):151833.
11. Chen K et al. Comprehensive insight into endothelial progenitor cell-derived extracellular vesicles as a promising candidate for disease treatment. 2022;13(1):238.
12. Yang J et al. Sevoflurane preconditioning promotes mesenchymal stem cells to relieve myocardial ischemia/reperfusion injury via TRPC6-induced angiogenesis. 2021;12(1):584.
13. Bahrami N, Ale-Ebrahim M. Combined application of human amniotic membrane mesenchymal stem cells and a modified PGS-co-PCL film in an experimental model of myocardial Ischemia-Reperfusion injury. Appl Biochem Biotechnol. 2023;195(12):7502–19.
14. Nguyen TH-N, Pham PV, Vu NB. Exosomes from adipose-derived stem cells promote angiogenesis and reduce necrotic grade in hindlimb ischemia mouse models. Iran J Basic Med Sci. 2023;26(4).
15. Sadri F, Rezaei Z, Fereidouni M. The significance of the SDF-1/CXCR4 signaling pathway in the normal development. Mol Biol Rep. 2022;49(4):3307–20.

16. Shi W et al. Neovascularization: the main mechanism of MSCs in ischemic heart disease therapy. Front Cardiovasc Med. 2021;8:633300. https://doi.org/10.3389/fcvm.2021.633300
17. Attar A, et al. Correction: Effect of once versus twice intracoronary injection of allogeneic-derived mesenchymal stromal cells after acute myocardial infarction: BOOSTER-TAHA7 randomized clinical trial. Stem Cell Res Ther. 2024;15(1):40.
18. Amini H, et al. Exosome-bearing Hydrogels Cardiac Tissue Regeneration. Biomater Res. 2023;27(1):99.
19. Samadi A, et al. Cell encapsulation and 3D Bioprinting for therapeutic cell transplantation. ACS Biomater Sci Eng. 2023 Apr 10;9(4):1862–1890.
20. Kim W, et al. Therapeutic strategies of three-dimensional stem cell spheroids and organoids for tissue repair and regeneration. Bioactive Mater. 2023;19:50–74.
21. Chang C, et al. Effects of mesenchymal stem cell-derived paracrine signals and their delivery strategies. Adv Healthc Mater. 2021;10(7):2001689.
22. Zheng Z, et al. Biotherapeutic-loaded injectable hydrogels as a synergistic strategy to support myocardial repair after myocardial infarction. J Controlled Release. 2021;335:216–36.
23. Łabowska MB, et al. A review on the adaption of Alginate-Gelatin hydrogels for 3D cultures and Bioprinting. Materials. 2021;14. https://doi.org/10.3390/ma14040858.
24. Amini H, et al. Cytoprotective and cytofunctional effect of polyanionic polysaccharide alginate and gelatin microspheres on rat cardiac cells. Int J Biol Macromol. 2020;161:969–76.
25. Zhang R, et al. Polyvinyl alcohol/gelatin hydrogels regulate cell adhesion and chromatin accessibility. Int J Biol Macromol. 2022;219:672–84.
26. Nemati S et al. The effect of alginate-gelatin encapsulation on the maturation of human myelomonocytic cell line U937. 2019;13(1):25–35.
27. Alizadeh Sardroud H, Khoshfetrat SNAB, Nabavinia M, Beygi Y, Khosrowshahi. Barium-crosslinked alginate-gelatin microcapsule as a potential platform for stem cell production and modular tissue formation. J Microencapsul. 2017;34(5):488–97.
28. Ben Fraj S, Naserian S. Hum Umbilical Cord Blood Endothelial Progenit Cell-Derived Extracell Vesicles Control Important Endothelial Cell Funct. 2023;24(12).
29. Hassanpour M, et al. A reversal of age-dependent proliferative capacity of endothelial progenitor cells from different species origin in in vitro condition. J Cardiovasc Thorac Res. 2016;8(3):102–6.
30. Hassanpour M, et al. Chronic exposure of human endothelial progenitor cells to diabetic condition abolished the regulated kinetics activity of exosomes. Iran J Pharm Res. 2018;17(3):1068–80.
31. Rahbarghazi R, et al. Dynamic induction of pro-angiogenic milieu after transplantation of marrow-derived mesenchymal stem cells in experimental myocardial infarction. Int J Cardiol. 2014;173(3):453–66.
32. Mathlouthi M. Vibrational spectra of carbohydrates. Adv Carbohydr Chem Biochem. 1986;44:7–89.
33. Silverstein RM. Spectrometric identification of organic compounds. J Chem Educ. 1962;39(11):546.
34. Chandıa N, Vásquez BMA. Alginic acids in Lessonia trabeculata: characterization by formic acid hydrolysis and FT-IR spectroscopy. Carbohydr Polym. 2001;46(1):81–7.
35. Hassani A, Rahbarghazi ABKR, Sakai S. Collagen and nano-hydroxyapatite interactions in alginate-based microcapsule provide an appropriate osteogenic microenvironment for modular bone tissue formation. Carbohydr Polym. 2022;277:118807.
36. Sarker B, Zehnder RST, Forgber T, Alexiou C, Cicha I, Detsch R, Boccaccini AR. Macromolecular interactions in alginate–gelatin hydrogels regulate the behavior of human fibroblasts. J Bioactive Compatible Polym. 2017;32(3):309–24.
37. Sharma C, Potdar AKDPD, Chou CF, Mishra NC. Fabrication and characterization of novel nano-biocomposite scaffold of chitosan–gelatin–alginate–hydroxyapatite for bone tissue engineering. Mater Sci Eng C. 2016;64:416–27.
38. Bouklas N. Swelling kinetics of polymer 807 gels: comparison of linear and nonlinear theories. Soft Matter. 2012;8(31):8194–203.
39. Smidsrød O. Molecular basis for some physical properties of alginates in the gel state. Faraday Discuss Chem Soc. 1974;57:263–74.
40. Okay O. General properties of hydrogels. Hydrogel Sens Actuators. 2009:1–14.
41. Salmieri S. Physicochemical properties of Alginate/Polycaprolactone-Based films containing essential oils. J Agric Food Chem. 2006;54(26):10205–14.
42. Gombotz WR. Protein release from alginate matrices. Adv Drug Deliv Rev. 1998;31(3):267–85.
43. Montalbano G, Popov STA, Duan P, Chen J, Dalgarno K, Scott WE 3rd, Ferreira AM. Synthesis of bioinspired collagen/alginate/fibrin based hydrogels for soft tissue engineering. Mater Sci Engineering: C. 2018;91:236–46.
44. Zhang J, Gauthier WLO, Sourice S, Pilet P, Rethore G, Khairoun K, Bouler JM, Tancret F, Weiss P. A simple and effective approach to prepare injectable macroporous calcium phosphate cement for bone repair: Syringe-foaming using a viscous hydrophilic polymeric solution. Acta Biomater. 2016;31:326–38.
45. Martinez AW, Ravi JMCS, Li W, Chaikof EL. Effects of crosslinking on the mechanical properties, drug release and cytocompatibility of protein polymers. Acta Biomater. 2014;10(1):26–33.
46. Hassani A, Kerdar ÇBASN, Amini H, Amini M, Ahmadi M, Sakai S, Bagca BG, Ozates NP, Rahbarghazi R, Khoshfetrat AB. Interaction of alginate with nano–hydroxyapatite–collagen using strontium provides suitable osteogenic platform. J Nanobiotechnol. 2022;20:310.
47. Takubo N, et al. Cohesive and anisotropic vascular endothelial cell motility driving angiogenic morphogenesis. Sci Rep. 2019;9(1):9304.
48. Pangjantuk A, et al. 3D culture of alginate-hyaluronic acid hydrogel supports the stemness of human mesenchymal stem cells. Sci Rep. 2024;14(1):4436.
49. Astaneh ME, et al. Chitosan/gelatin hydrogel and endometrial stem cells with subsequent Atorvastatin injection impact in regenerating spinal cord tissue. J Drug Deliv Sci Technol. 2020;58:101831.
50. Liao S, et al. Injectable adipose-derived stem cells-embedded alginate-gelatin microspheres prepared by electrospray for cartilage tissue regeneration. J Orthop Translation. 2022;33:174–85.
51. Yang L, et al. Chitin-based hydrogel loaded with bFGF and SDF-1 for inducing endogenous mesenchymal stem cells homing to improve stress urinary incontinence. Carbohydr Polym. 2023;319:121144.
52. Cun Y, et al. Role of the stromal cell derived factor–1 in the biological functions of endothelial progenitor cells and its underlying mechanisms. Exp Ther Med. 2021;21(1):39.
53. Ge Q, et al. VEGF secreted by mesenchymal stem cells mediates the differentiation of endothelial progenitor cells into endothelial cells via paracrine mechanisms. Mol Med Rep. 2018;17(1):1667–75.
54. Saberianpour S et al. Juxtaposition of mesenchymal stem cells with endothelial progenitor cells promoted angiogenic potential inside Alginate-Gelatin microspheres. Adv Pharm Bull. 2021;11(1):163–70. https://doi.org/10.34172/apb.2021.017
55. Guan YT, et al. Comparison of biological characteristics of mesenchymal stem cells derived from the human umbilical cord and decidua parietalis. Mol Med Rep. 2019;20(1):633–9.
56. Trouche E, et al. Evaluation of alginate microspheres for mesenchymal stem cell engraftment on solid organ. Cell Transpl. 2010;19(12):1623–33.
57. Rizzo M et al. IL-8 and its role as a potential biomarker of resistance to anti-angiogenic agents and immune checkpoint inhibitors in metastatic renal cell carcinoma. Front Oncol. 2022;12:990568.
58. Damås JK, et al. Stromal Cell–Derived Factor-1α in unstable angina. Circulation. 2002;106(1):36–42.
59. Choi J, et al. FGF2-primed 3D spheroids producing IL-8 promote therapeutic angiogenesis in murine hindlimb ischemia. Npj Regenerative Med. 2021;6(1):48.
60. Herberg S, et al. Stromal cell-Derived Factor-1β mediates cell survival through enhancing autophagy in bone Marrow-Derived mesenchymal stem cells. PLoS ONE. 2013;8(3):e58207.
61. Li J, et al. SDF-1α promotes chondrocyte autophagy through CXCR4/mTOR signaling Axis. Int J Mol Sci. 2023;24. https://doi.org/10.3390/ijms24021710.
62. Wang S, et al. Exogenous stromal cell-derived factor-1 (SDF-1) suppresses the NLRP3 inflammasome and inhibits pyroptosis in synoviocytes from Osteoarthritic joints via activation of the AMPK signaling pathway. Inflammopharmacology. 2021;29(3):695–704.
63. Tang J, et al. Sequestosome 1/p62: A multitasker in the regulation of malignant tumor aggression (Review). Int J Oncol. 2021;59(4):77.
64. Ma S, Attarwala IY, Xie XQ. SQSTM1/p62: A potential target for neurodegenerative disease. ACS Chem Neurosci. 2019;10(5):2094–114.
65. Yin J, et al. Angiopoietin 2 promotes angiogenesis in tissue-engineered bone and improves repair of bone defects by inducing autophagy. Biomed Pharmacother. 2018;105:932–9.
66. Hassanpour M, et al. Autophagy modulation altered differentiation capacity of CD146 + cells toward endothelial cells, pericytes, and cardiomyocytes. Stem Cell Res Ther. 2020;11(1):139.
67. Zhang B, et al. Essential contribution of macrophage Tie2 signal mediated autophagy in laser-induced choroidal neovascularization. Exp Eye Res. 2020;193:107972.

68. Döring Y, et al. Vascular CXCR4 limits atherosclerosis by maintaining arterial integrity: evidence from mouse and human studies. Circulation. 2017;136(4):388–403.
69. Grimsley-Myers CM et al. VE-cadherin endocytosis controls vascular integrity and patterning during development. J Cell Biol. 2020;219(5).
70. Liu Y, et al. Stem cells in the treatment of renal fibrosis: a review of preclinical and clinical studies of renal fibrosis pathogenesis. Stem Cell Res Ther. 2021;12(1):333.
71. Gubert F, et al. Mesenchymal stem cells therapies on fibrotic heart diseases. Int J Mol Sci. 2021;22(14):7447.
72. Raman N, et al. Mechanotransduction of mesenchymal stem cells (MSCs) during cardiomyocytes differentiation. Heliyon. 2022;8(11):e11624.
73. Bajdak-Rusinek K, Fus-Kujawa A. SDF-1α-releasing microspheres effectively extend stem cell homing after myocard infarct. Biomedi. 2023;11(2):343.
74. Prabahar A, et al. Unraveling the complex relationship between mRNA and protein abundances: a machine learning-based approach for imputing protein levels from RNA-seq data. NAR Genomics Bioinf. 2024;6(1):lqae019.
75. Urbach C, et al. Combinatorial screening identifies novel promiscuous matrix metalloproteinase activities that lead to Inhibition of the therapeutic target IL-13. Chem Bio 2015;22(11):1442–52.
76. Kim YI, et al. Reduced matrix metalloproteinase and collagen transcription mediated by the TGF-β/Smad pathway in passaged normal human dermal fibroblasts. J Cosmet Dermatol. 2020;19(5):1211–8.
77. Lozito TP, et al. Human mesenchymal stem cells generate a distinct pericellular zone of MMP activities via binding of MMPs and secretion of high levels of timps. Matrix Biol. 2014;34:132–43.
78. Tkacz M, et al. Responses of endothelial progenitor cells to chronic and acute physical activity in healthy individuals. Int J Mol Sci. 2024;25. https://doi.org/10.3390/ijms25116085.
79. Yun WS et al. Fluorescence-based mono- and multimodal imaging for in vivo tracking of mesenchymal stem cells. Biomol. 2023;13. https://doi.org/10.3390/biom13121787
80. Prockop DJ, Oh JY, Lee RH. Data against a common assumption: xenogeneic mouse models can be used to assay suppression of immunity by human MSCs. Mol Ther. 2017;25(8):1748–56.
81. Abd E, Aziz MT, et al. Endothelial progenitor cells regenerate infracted myocardium with neovascularisation development. J Adv Res. 2015;6(2):133–44.

Publisher's note